ENSO Influence on Western European Summer and Fall Temperatures

MAIALEN MARTIJA-DÍEZ,[a,b] BELÉN RODRÍGUEZ-FONSECA,[b,c] AND JORGE LÓPEZ-PARAGES[d]

[a] *TECNALIA, Basque Research and Technology Alliance, Vitoria-Gasteiz, Spain*
[b] *Departamento de Física de la Tierra y Astrofísica, Universidad Complutense de Madrid, Spain*
[c] *Instituto de Geociencias IGEO, CSIC UCM, Spain*
[d] *Physical Oceanography Group, University of Málaga, Málaga, Spain*

(Manuscript received 20 October 2020, in final form 9 July 2021)

ABSTRACT: In certain regions, such as Europe, the increase in global air temperatures in the world is translated into more frequent extreme events. Recent studies suggest that the increasing intensity in heatwaves seems to be related to the interannual variability of the mean temperature, a finding that motivates the search for its possible predictability. El Niño–Southern Oscillation (ENSO) is the principal predictor of global climate variability at interannual time scales. Its impact on European climate has been deeply studied in relation to rainfall variability, but only a few studies exist that focus on its impact on temperature. In this work, we focus on the analysis of the interannual variability of maximum and minimum temperatures in order to find some predictability and trends. To that end, we choose the western European region, which has experienced intense heatwaves and is also the main region of air temperature interannual variability in Europe. Our results indicate that the ENSO impact on temperatures over this region is nonlinear and nonstationary. We have found the way in which, during the decades prior to 1980s, the increase in temperatures is related to La Niña in summer and to El Niño in fall during the decades after the 1980s, which shows a change in the seasonality of the impact. We study the dynamical mechanisms involved, which suggest a circumglobal response for summer and an arching-like teleconnection pattern in fall. The aforementioned warmer conditions in western European temperatures are found to be significantly correlated to ENSO characteristics of previous seasons, which suggests a potential source for improving the seasonal forecast.

KEYWORDS: ENSO; Teleconnections; Climate variability; Sea surface temperature

1. Introduction

The increase in global surface temperature is one of the most evident fingerprints of climate change, having strong impact over Europe, especially in summer (Giorgi 2006; Fischer et al. 2014; Bador et al. 2017). In particular, western and central Europe have been affected by extreme heatwaves during recent years (Kyselý 2010; García-Herrera et al. 2010; Barriopedro et al. 2011), and it is believed that they will become more frequent, more intense, and longer-lasting under climate change scenarios (Guerreiro et al. 2018). In particular, the temperature during the summer of 2003 exceeded that of any previous summer over the preceding 500 years (Trigo et al. 2005), and the heatwave between 1 and 15 August was regarded as the deadliest natural disaster during last 50 years in Europe (De Bono et al. 2004). Most recently, in June 2017, extremely high temperatures were detected in western Europe (WE), giving rise to the warmest June in Iberia and the second warmest recorded in France and Switzerland (Sánchez-Benítez et al. 2018). A recent study has found how the hot summers of 2017 and 2018 in the Northern Hemisphere could be related not only to global warming but also to natural internal variability (Zheng and Wang 2019).

Research into the ways that such high temperatures can be better predicted is vital for reducing the socioeconomic impacts of future heatwaves (Della-Marta et al. 2007). The increasing intensity of heatwaves seems to be a consequence of higher mean temperatures (Ballester et al. 2010), which suggests that improving the predictability of anomalous summer mean air temperatures will help to forecast the heatwaves that are probably related to them (Ossó et al. 2018).

It is well known that European climate variability can be associated with both atmospheric internal variability and sea surface temperature (SST)-forced atmospheric teleconnections, not only from the surrounding oceans but also from remote regions such as the Pacific Ocean (Hoerling et al. 2001, 2004; Bracco et al. 2004; Hurrell et al. 2004; Branstator and Selten 2009; Deser and Phillips 2009; Hurrell and Deser 2009). Nevertheless, the mechanism, linearity, timing, and stationarity of these teleconnections throughout the seasonal cycle are still a matter of debate (López-Parages et al. 2015, 2016, hereafter LP15, LP16; Rodríguez-Fonseca et al. 2016; Brands 2017; Bulić et al. 2017).

Regarding forced response, several studies point to El Niño–Southern Oscillation (ENSO) as a mode of variability with a modest but significant impact on the North Atlantic–European sector (NAES; Brönnimann 2007; Rodríguez-Fonseca et al. 2016; Taschetto et al. 2020). This influence of ENSO has been related to an atmospheric dipole pattern that resembles the North Atlantic Oscillation (NAO; Mezzina et al. 2020), identifying a link between the positive ENSO phase and a negative NAO-like pattern, mainly during boreal wintertime (e.g., Pozo-Vázquez et al. 2005; García-Serrano et al. 2011).

Supplemental information related to this paper is available at the Journals Online website: https://doi.org/10.1175/JCLI-D-20-0808.s1.

Corresponding author: Maialen Martija-Díez, maialen.martija@tecnalia.com

DOI: 10.1175/JCLI-D-20-0808.1

However, different ENSO spatial configurations trigger distinct teleconnections and responses over the European continent (Frauen et al. 2014; LP16).

Furthermore, the linearity (or not) of the influence of La Niña (LN) and El Niño (EN) over Europe is not yet completely understood, as contradictory results are reported in the literature (Deser et al. 2017; Ayarzagüena et al. 2018a). This influence has been found to be nonstationary in time, indicating that the Atlantic multidecadal variability (AMV) is a modulator of the ENSO signature in central Europe and WE (López-Parages and Rodríguez-Fonseca 2012, hereafter LP12). Some modulations associated with the Pacific decadal oscillation (PDO) have also been described (Zanchettin et al. 2008; LP12; Zhang et al. 2012; LP15, LP16). Nevertheless, the multidecadal modulation of ENSO impact on Europe still requires more research, even more so where the expected changes due to global warming are concerned (Müller and Roeckner 2008).

The role of the ENSO diversity on the associated teleconnections is also under debate (Taschetto et al. 2020). Distinct spatial ENSO patterns [eastern Pacific (EP) vs central Pacific (CP)], linked to different position of the SST anomalies in the equatorial Pacific, seem to impact the Pacific atmosphere differently, and in turn to modify the Rossby waves affecting the European climate (LP16).

For more in-depth research into the socioeconomic impacts associated with the ENSO–WE teleconnection, it is important to address the signatures on fundamental meteorological variables, such as surface temperature and rainfall. Significant responses to ENSO for European rainfall (Stockdale et al. 1998; Raible et al. 2003; Shaman and Tziperman 2011; Bulić and Kucharski 2012; Shaman 2014a,b) and temperature (Bergman 1984; Kiladis and Diaz 1989) have been documented, although the latter has been less studied.

Although a stratosphere pathway has also been reported (Manzini et al. 2006; Bell et al. 2009; Cagnazzo and Manzini 2009; Ineson and Scaife 2009; Ayarzagüena et al. 2018b), the main mechanism explaining the ENSO teleconnection with the NAES is through tropospheric Rossby waves generated by anomalous diabatic heating in the tropical Pacific. This mechanism can be viewed as a combination of an arching-like pattern and a circumglobal teleconnection pattern (CGT; Branstator 2002) trapped along the northern jet stream (Lau and Peno 1992; Chen 2002; Ding et al. 2011, hereafter D11). Regarding the former, two different arching teleconnection structures reaching the North Atlantic from the tropical Pacific have been described: the Pacific–North American (PNA) pattern and the tropical Northern Hemisphere (TNH) pattern (Mo and Livezey 1986; Barnston et al. 1991). The TNH, which shifts eastward with respect to the PNA, has mostly been related to ENSO, in contrast to the PNA, which can also be internally generated (Bonsal and Shabbar 2011). In this context, and focusing on wintertime, Yu et al. (2015) show that the PNA-type teleconnection seems to come from both EP and CP ENSO patterns, while the TNH pattern comes from EP ENSO spatial configurations. Furthermore, Brönnimann (2007) found how the TNH-type teleconnection pattern is limited to winter and it is not until January when this spatial structure is completely established (Bladé et al. 2008; King et al. 2018). In relation to the CGT teleconnection, the ENSO-forced response has been described as a wavenumber-5 structure (Ding and Wang 2005, hereafter DW05). Most of the aforementioned studies are focused on winter, when ENSO reaches its peak. However, D11 analyze the tropical–extratropical teleconnection in summers before and after ENSO episodes, concluding that CGT dominates in summers before the event's peak and the arching-like pattern in summers after it.

In this work, we focus on the ENSO teleconnection with the European air surface temperatures, with particular attention to the related impact on maximum and minimum temperatures (Tmax and Tmin) over WE. The possible nonstationary and nonlinear features of the teleconnection have also been addressed.

The structure of the manuscript is as follows. In section 2, data and methodology are described. Section 3 presents the results, starting with a brief explanation of the seasonal cycle of Tmax and Tmin in WE, followed by an analysis of the ENSO influence on this area, and finishing with a potential application of our results to improve seasonal predictability. Finally, a summary and a brief discussion are presented in section 4.

2. Data and methods

In this work, a daily high-resolution gridded dataset (E-OBS 17.0; Cornes et al. 2018), with 0.25° × 0.25° latitude–longitude resolution, is used for analyzing the variability of Tmax and Tmin over WE (35°–63°N, 10°W–6°E). Additionally, different atmospheric and oceanic reanalysis datasets are selected in order to explore the associated dynamical mechanisms. The period chosen is 1950–2016 (referred to simply as the whole period of analysis).

The atmospheric variables come from the gridded NCEP–NCAR reanalysis (Kalnay et al. 1996) with 2.5° × 2.5° latitude–longitude resolution. In particular, we use temperature at 850 hPa (T850) over the NAES (30°–70°N, 60°W–20°E), and geopotential height and zonal wind velocity at 200 hPa (Z200 and U200), all in the tropical band and the Northern Hemisphere (30°S–90°N, 0°–360°E).

The SST comes from the Hadley Centre Sea Ice and Sea Surface Temperature dataset (HadISST; Rayner et al. 2003), which covers the globe with a grid of 1° × 1° latitude–longitude resolution. This dataset is also used for calculating distinct EN indices: Niño-1.2 (10°S–0, 90°–80°W), Niño-3 (5°S–5°N, 150°–90°W), Niño-3.4 (5°S–5°N, 170°–120°W), and Niño-4 (5°S–5°N, 160°E–150°W).

Throughout this study, distinct anomaly correlation analysis are performed to investigate the link between Tmax and Tmin in WE and the tropical Pacific SSTs associated with ENSO. In particular, we address the stationarity of this teleconnection by calculating these correlations in a 20-yr sliding window and, since we focus on interannual time scales, a high-pass Butterworth filter (with a cutoff threshold of 7 years) is applied to the anomalous fields.

An empirical orthogonal function (EOF) analysis is also applied to study in depth the variability of Tmax and Tmin in WE. To this end, we calculate the temporal variances of these variables for all the spatial points within WE and analyze the regions sharing variability. The resultant variance matrix is diagonalized, and the principal directions (EOFs) in which the

variability is organized are represented in terms of correlation maps between the corresponding principal component and the Tmax and Tmin anomalies at each spatial point (von Storch and Zwiers 2001). We also obtain the different composite maps based on Tmax, Tmin, and EN indices. Composites of geopotential height at upper levels are represented in order to address the teleconnection mechanisms with ENSO.

With the aim of better understand the underlying mechanisms involved in the teleconnection, the outgoing longwave radiation (OLR), and the atmospheric streamfunction and the wave activity flux (WAF) at the upper troposphere are also computed. The latter, which broadly represents the group velocity of Rossby waves, is computed from the anomalous wind components and the zonally asymmetric part of the streamfunction regression maps [assuming stationary Rossby waves and neglecting vertical movements; see Eq. (38) of Takaya and Nakamura (2001) for further details]. This magnitude can be very useful when analyzing the migratory and stationary disturbances propagating through a zonally varying basic flow.

Through the whole study, we analyze the statistical significance using a Student's t test. An alternative Fisher's f test is applied for the significance of the standard deviation (std) and a Monte Carlo tests for cases with poor significance, as for the streamfunction and the WAF (1000 permutations of the original data). In all cases, a 90% confidence level is chosen.

3. Results

To examine changes in Tmax and Tmin during the observed period and following its seasonal cycle, a region in WE has been selected (WE-box; see the black box in Fig. 1). This subdomain represents a significant center of action of Tmax and Tmin variability (Fig. 1). The corresponding leading EOFs explain around the 50% of the total variance, thus highlighting its relevance in terms of interannual variability. We use the target area within the selected box in order to create related indices (the Imax index by averaging Tmax over the WE-box and the Imin index by averaging Tmin over the WE-box).

In section 3a, we analyze the seasonal cycle of Tmax and Tmin in the region under study (WE-box), including possible nonstationarities. We analyze this aspect further in sections 3b and 3c with the aim of determining the possible modulating role of the changing climatological conditions. ENSO impact throughout the seasonal cycle is assessed by calculating a 20-yr moving-window correlation, for each season, between the Imax and Imin indices and different EN indices (section 3b). This enables us to address the seasonality and the stationarity of the teleconnection as well as the role of ENSO in terms of spatial (EP and CP spatial configurations) and temporal (EN vs LN phases) nonlinearities.

a. Seasonal cycle

Considering the whole period of 1950–2016, Imax and Imin present their maximum and minimum mean values during boreal summer and winter, respectively (Figs. 2a,b). Regarding variability, both variables present the highest variability in the coldest season, with a secondary relative maximum for Imax in summer. On the other hand, the lowest variability appears in fall for Imax and in late summer for Imin.

To deepen the evolution of the seasonal cycle, we perform a 20-yr sliding-window analysis (Figs. 2c,d). The mean anomalies in Imax (Fig. 2c) and Imin (Fig. 2d) show a clear tendency to highest values in the last decades of the whole period, in agreement with the evolution of global warming over the region (Vicente-Serrano and Rodríguez-Camino 2017). Changes in variability (Figs. 2e,f) show maximum values that seem to change from winter during the early 1960s to spring around the 1980s and finishing at fall in the 2000s. Nevertheless, most of these values are not statistically significant and should be interpreted with caution.

b. ENSO influence

To explore the possible role of ENSO in modifying the interannual variability of temperature in our study region, we calculate a 20-yr moving-window correlation between two WE anomalous Imax and Imin indices (calculated by removing the seasonal mean of the whole period) and different EN indices. These correlations are performed for all the possible 3-month seasons of the year, from JFM (January–March) to DJF (December–February). Since the ENSO teleconnections may change according to the location of the Pacific SST anomalies (Frauen et al. 2014; LP15, LP16; Zhang et al. 2019), different EN indices are used for considering distinct ENSO flavors (EP vs CP).

The results point to summer and fall as the seasons in which ENSO impacts on temperature, showing negative correlations in the former season and positive correlations in the latter. These values exceed 0.5 in OND and reach −0.7 for JAS (Fig. 3). Nevertheless, these peaks occur in particular periods and the statistical significance is limited to some specific decades for the selected box, indicating a remarkable nonstationary relationship with ENSO. The decades in which a stronger signal is detected agree with those found in LP12 when analyzing rainfall, in which correlations between ENSO and rainfall turned from negative to positive values in the mid-1970s. This changing teleconnection could be linked to the so-called climate shift that took place in the Pacific in 1976 (Venrick et al. 1987; Ebbesmeyer et al. 1991), but also with variations in the AMV (with changes of phases in 1968 and 1995; Knight et al. 2006) and/or the anthropogenic global warming (IPCC 2014).

Surprisingly, no significant correlations appear between Imax and Imin and EN indices in winter and spring, seasons that have been proposed as those with stronger ENSO impacts on Europe (e.g., LP12; Shaman 2014b). This finding should be interpreted not as an absence of the ENSO teleconnection with Europe in these seasons, but rather as an absence of ENSO impact on temperature, since most of the previous studies focused on rainfall.

The pattern of positive correlations with ENSO shown in Fig. 3 (please see the yellow/red shaded areas) changes from winter in the 1960s to summer in the 1980s, ending in fall during the 2000s, when the correlations become significant for almost all the EN flavors (except for Niño-1.2 and Niño-3 with Tmax). This structure presents some similarities with those in the seasonal cycle variability represented in Fig. 2. Indeed, the periods and seasons with higher correlations and higher std broadly coincide, despite the absence of significance. This concomitance reinforces the hypothesis of ENSO as an important driver behind the changes in the seasonal cycle.

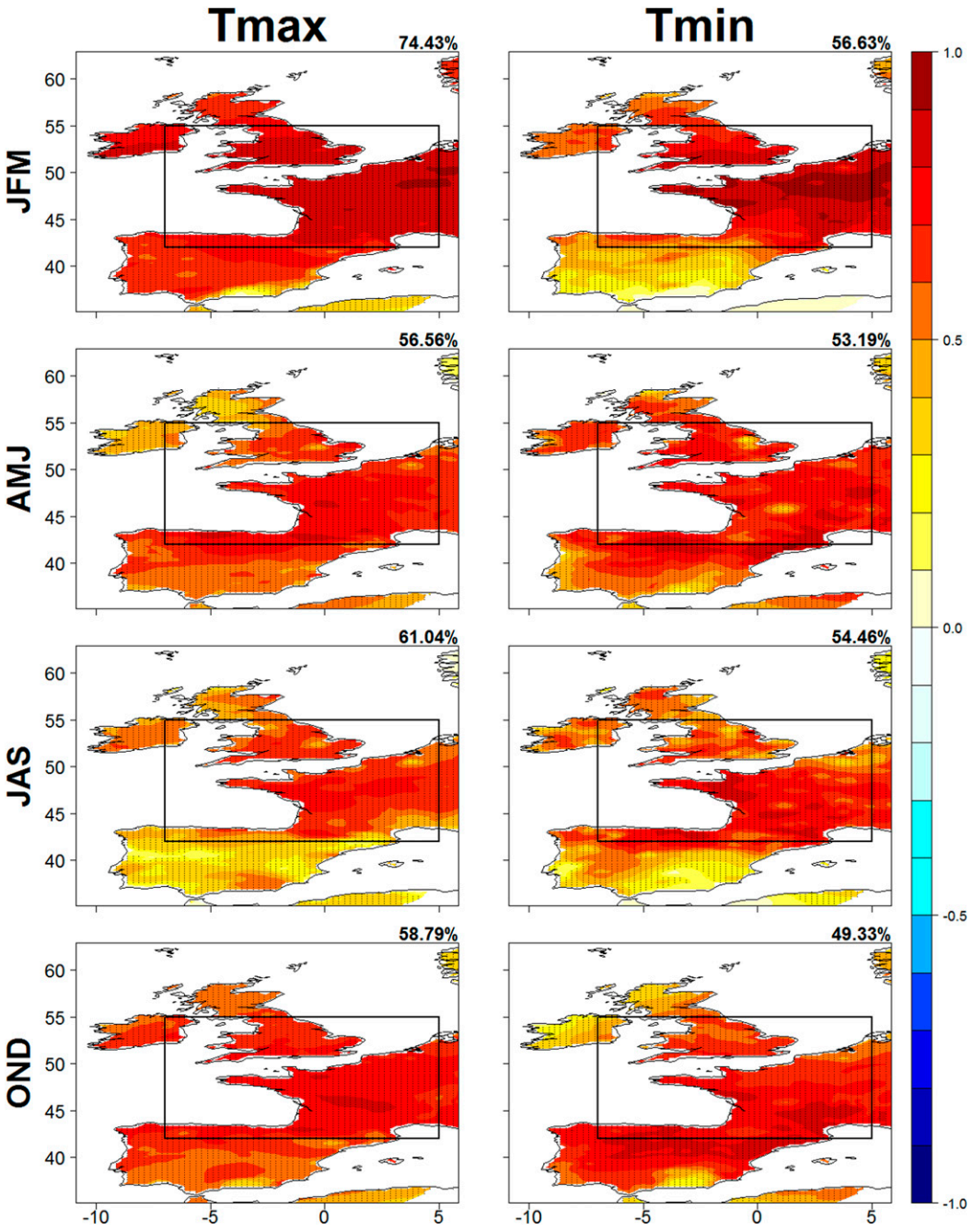

FIG. 1. Leading modes of Tmax and Tmin variability in WE. Leading empirical orthogonal function (EOF1) [contours, contour interval (ci) = 0.1° per std in the PC] of the anomalous temperature over WE (35°–63°N, 10°W–6°E). The percentage of explained variance is indicated in the right-hand corner of each panel. Dotted regions indicate statistically significant areas, according to a *t* test at the 90% level of confidence. The black box indicates the domain (WE-box; 42°–55°N, 7°W–5°E) used to create a Tmax and Tmin index (Imax and Imin) in the present study.

Another interesting feature is the sensitivity of the above-mentioned correlations with respect to the ENSO flavor (EP vs CP). The link identified in fall from the 1990s onward is stronger for the central tropical Pacific SSTs (Niño-3.4 and Niño-4) than for the eastern tropical Pacific SSTs (Niño-1.2 and Niño-3). On the other hand, the link in summer, although stronger for Niño-3 and Niño-3.4 indices, seems to be less sensitive to the ENSO spatial configuration.

The results in Fig. 3 point therefore to a seasonal and nonstationary ENSO teleconnection with WE temperatures. Thus, correct prediction of ENSO teleconnections with WE temperatures would require a deep analysis of the related seasonality and stationarity.

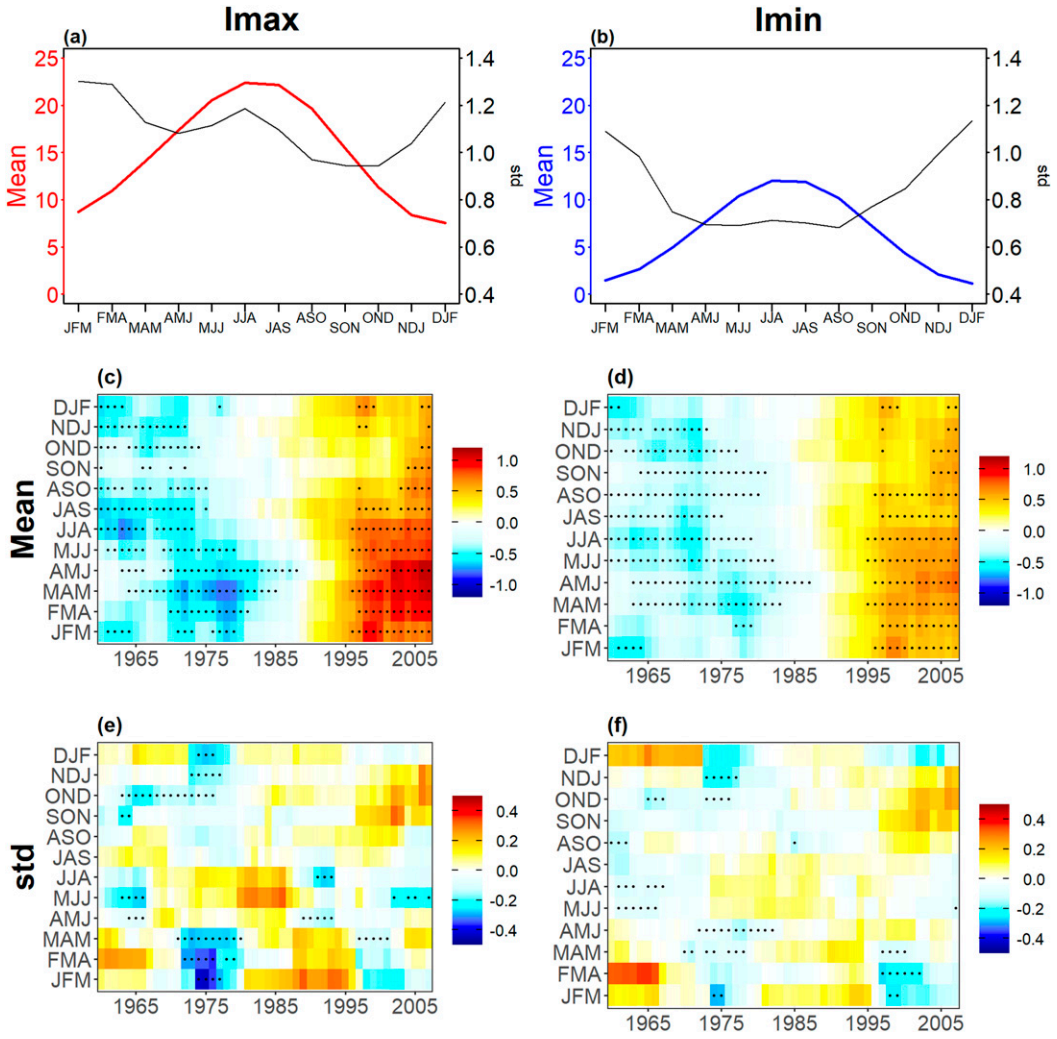

FIG. 2. Seasonal cycle of Imax and Imin: (a),(b) 3-month seasonal mean (left axis) and std (right axis) from 1950 to 2016. Also shown are 20-yr sliding-window (centered) seasonal means anomalies and std for (c),(e) Imax and (d),(f) Imin throughout the seasonal cycle. The dotted grid points indicate periods and seasons for which the mean (std) is significantly different from the mean (std) in the whole period in (a) and (b), according to a Student's *t* test (Fisher's *f* test) at the 90% confidence level. Box analyzed (WE-box) is 42°–55°N, 7°W–5°E.

The way in which the anomalous energy release from the ocean during different ENSO events occurs, and how it is propagated into the NAES, must be analyzed in order to check the physical robustness of all these statistical correlations. In addition, the causes of the changing teleconnection also require clarification. To this end, in section 3c we focus on the seasons and periods with significant correlations with ENSO: 1953–75 in summer [July–September (JAS)] and 1990–2016 in fall [October–December (OND)]. The linearity of the teleconnection will be also addressed.

c. *Teleconnections in summer and fall*

1) SUMMER (JAS; 1953–75)

ENSO teleconnections with Europe are not only nonstationary, but also nonlinear in terms of spatial structure (LP16). Nevertheless, the linearity (or not) in terms of ENSO phase is still under debate (Deser et al. 2017; Ayarzagüena et al. 2018a). To gain a preliminary idea of how each phase of ENSO (EN and LN) impacts temperature within WE, and to compare these, we show a year-by-year evolution of Imax, Imin, and Niño-3.4 indices (Fig. 4). Although statistically significant correlations appear in Fig. 3 for all EN indices (suggesting a minor dependence with ENSO flavor), the strongest ones are obtained for Niño-3.4. As a consequence, we used this EN index in Fig. 4.

In the selected period (1953–75), Imax/Imin and Niño-3.4 present an opposite evolution, in congruence with the negative correlations shown in Fig. 3. Twelve of the 23 years analyzed present opposite anomalies between Imax and Niño-3.4, and eight between Imin and Niño-3.4 (black dots). A total of 16 ENSO events take place during this period (in green; 4 EN cases denoted as + and 12 LN cases denoted as −), showing

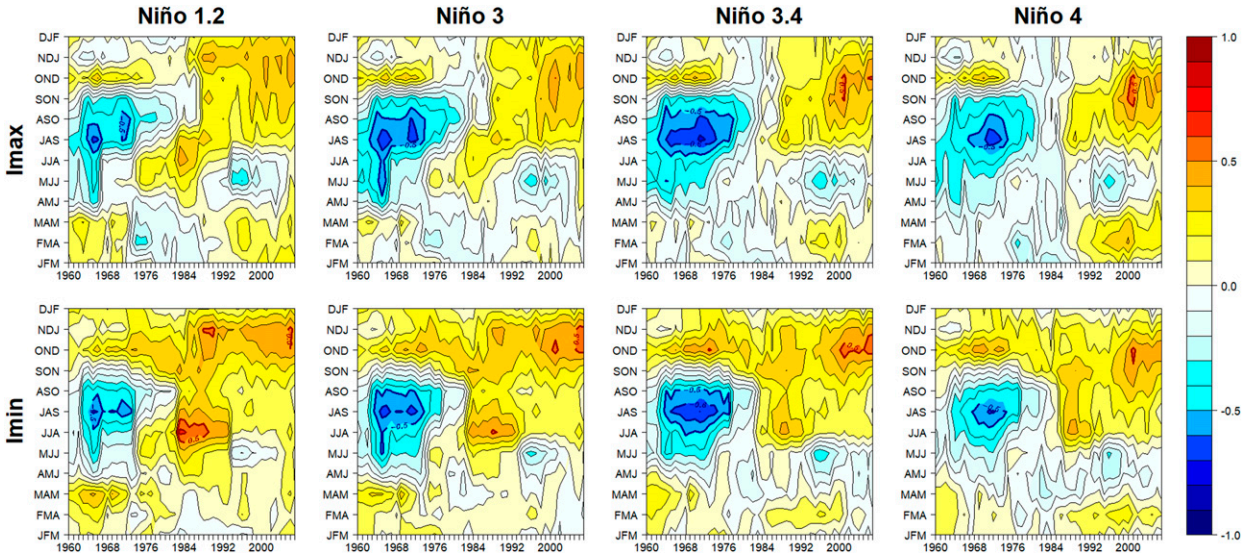

FIG. 3. Variability in seasonal cycle of ENSO correlations with Imax and Imin. Evolution of the 20-yr window (centered) correlation (sliding 1 year, from 1950 to 2016) between (top) Imax and (bottom) Imin and the indices of (from left to right) Niño-1.2, Niño-3, Niño-3.4, and Niño-4. The correlation is calculated for the 12 possible 3-month seasons of the year and all 20-yr windows. The bold contours correspond to statistically significant values, according to a t test at the 90% confidence level. From this figure, the periods 1953–75 and 1990–2016 have been chosen as those with significant correlations with ENSO in summer (JAS) and fall (OND), respectively.

how 75% (50%) of the ENSO events have a significant impact on Tmax (Tmin). On the other hand, although the 1976–2016 period is even longer than 1953–75, this anticorrelation between Niño-3.4 and Imax/Imin appears noticeably weaker; with only 6 years out of 22 ENSO events matching that condition (black dots), less than 30% of the cases analyzed.

To explore the linearity of ENSO impact on WE, we performed a composite analysis for different variables in such a way that not only the direct impact on temperature, but also the associated teleconnection mechanisms can be addressed (Figs. 5–7). For simplicity, we hereafter refer to these composites of positive Imax and Imin anomalies as WARM (Figs. 5a–h) and

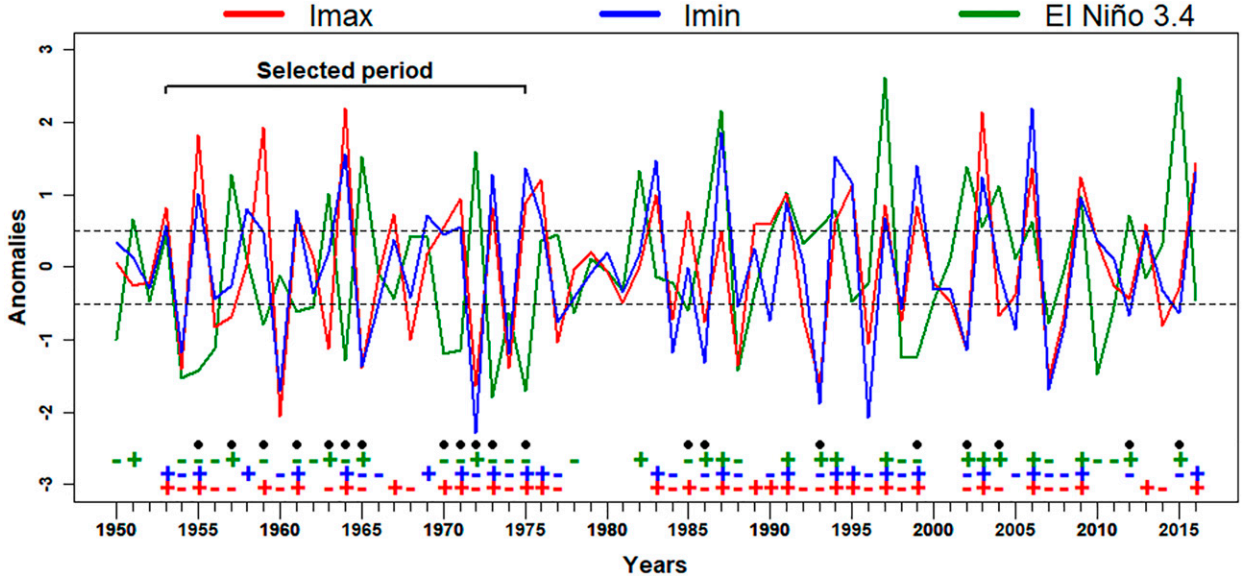

FIG. 4. JAS standardized anomalies of Imax (red), Imin (blue), and Niño-3.4 (green) indices throughout the whole period (1950–2016). The horizontal black dashed lines indicate thresholds (±0.5 std). Years that exceed the positive threshold for Imax, Imin, and Niño-3.4 are indicated in the bottom with red, blue, and green plus signs (+), respectively. The years that exceed negative threshold for Imax, Imin, and Niño-3.4 are indicated in the bottom with red, blue, and green minus signs (−), respectively. The black points represent the years that contribute to negative correlation between Niño-3.4 and Imax and/or Imin (positive/negative Niño and negative/positive Imax or Imin).

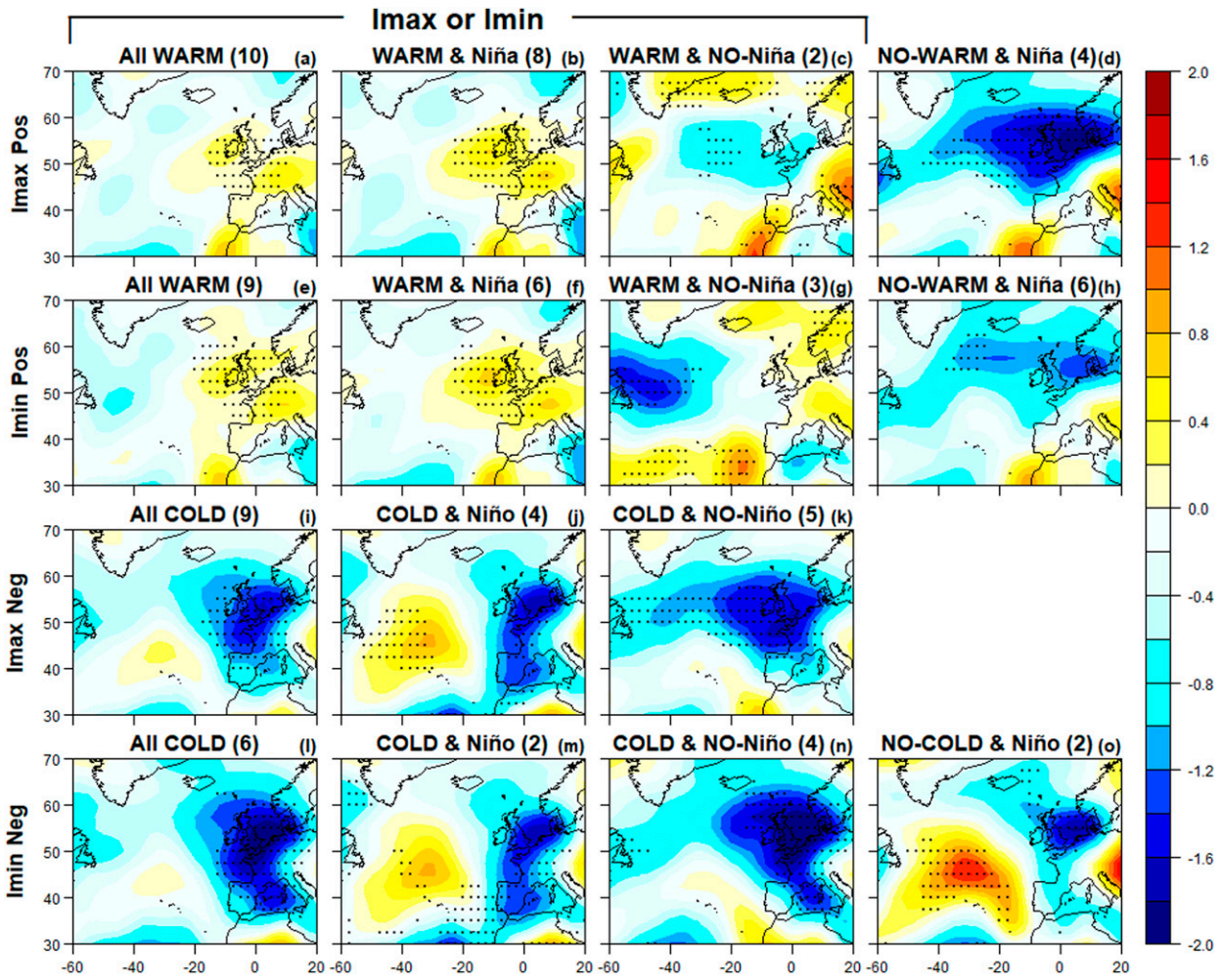

FIG. 5. Composites of T850 patterns and their relationship with ENSO in JAS. Composites of anomalous temperature at 850 hPa calculated for years with extreme Imax and Imin and considering Niño-3.4 influence throughout the period 1953–75 (selecting cases with standardized anomalies above 0.5 or below −0.5 std). Years corresponding to positive composites of (a) Imax and (e) Imin (WARM cases) are divided into years with (b),(f) negative Niño-3.4 index and (c),(g) no La Niña. (d),(h) Composites for negative Niño-3.4 events that do not match with WARM cases. (i)–(o) As in (a)–(h), but for the negative composites of (i) Imax and (l) Imin (COLD cases) and (j),(k),(m),(n) comparing with the positive composite of Niño-3.4 index and (o) showing the positive Niño-3.4 events that do not match with the COLD cases of Imin. The dotted regions indicate statistically significant areas according to a *t* test at the 90% confidence level.

to those of negative Imax and Imin as COLD (Figs. 5i–o), respectively. Furthermore, to further investigate the ENSO characteristics underlying the teleconnection, we isolate those ENSO years impacting WE temperatures (second column in Fig. 5) from those without an influence (right column in Fig. 5).

An initial result indicates how most WARM cases (8 out 10 for Imax and 6 out 9 for Imin) coincide with LN years (Figs. 5b,f). These cases present a center of positive anomalies over WE, which explains the warm surface temperature. On the contrary, the patterns associated with WARM events that are not related to LN (Figs. 5c,g) show weaker anomalies, suggesting therefore a totally different underlying mechanism. Strikingly, the remaining LN episodes (those unrelated to WARM events) present very cold and significant anomalies over WE (Figs. 5d,h). Thus, we identify apparent opposite impacts of LN in our study domain: one producing warm conditions (Figs. 5b,f) and other producing negative conditions (Figs. 5d,h). This suggests differences in LN characteristics and/or the underlying propagation mechanism. This feature is analyzed in depth in section 4.

For COLD cases (Figs. 5i–o), the relation to EN is not as clear as for WARM, since in less than half of cases (Figs. 5i,l) there is a concomitance with EN years (Figs. 5j,m). Furthermore, the negative anomalies over WE for those years with an EN event, although significant, extend through very limited areas (Figs. 5j,m). However, the patterns linked to COLD events and not related to EN show a marked negative center over WE (Figs. 5k,n). This suggests the presence of another source of predictability (apart from EN) behind these COLD events and/or an important impact of

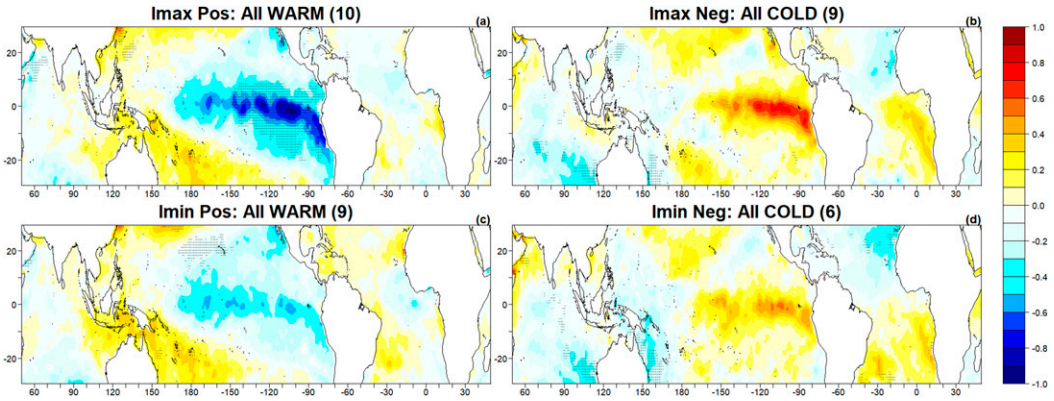

FIG. 6. Anomalies around the equator in JAS: SST anomalous composites for years with positive and negative extreme of (a),(b) Imax and (c),(d) Imin throughout the period 1953–75 [selecting cases with standardized anomalies (a),(c) above 0.5 std and (b),(d) below −0.5 std]. The dotted regions indicate statistically significant areas, according to a *t* test at the 90% confidence level.

internal variability in this case. Nevertheless, although EN could act as a predictor of COLD events, the sample available is very limited so we must be cautious when assessing predictability in these cases.

To arrive at a better assessment of the effect of ENSO flavor on WE temperatures, SST composites are obtained for WARM and COLD events over the tropical band (Fig. 6). As expected, WARM cases reveal a LN pattern extending over the eastern and central equatorial Pacific (Figs. 6a,c). This result is especially marked for Imax (Fig. 6a). For COLD cases, an EN signal emerges, especially for Imax, but it is not statistically significant. The same analysis but for the period with nonsignificant correlations between ENSO and Imax/Imin is presented in the online supplemental material (see Fig. S1 therein). As expected, the SST anomalies do not present any ENSO pattern.

Thus, our results suggest a robust relation between LN and WARM events. As a result, we focus on analyzing the teleconnection mechanism triggered by LN. Regarding the EN link with COLD events, given that only a small number of cases have been identified, no clear conclusions can be drawn (Figs. S2 and S3).

To address the mechanisms behind LN-related teleconnections, WARM composites are calculated for both global SST and Z200 (Fig. 7). The climatological jet stream over the Northern Hemisphere is also represented by plotting the zonal wind at the same level (U200). This is done to determine the role of the jet stream intensity and configuration in propagating the

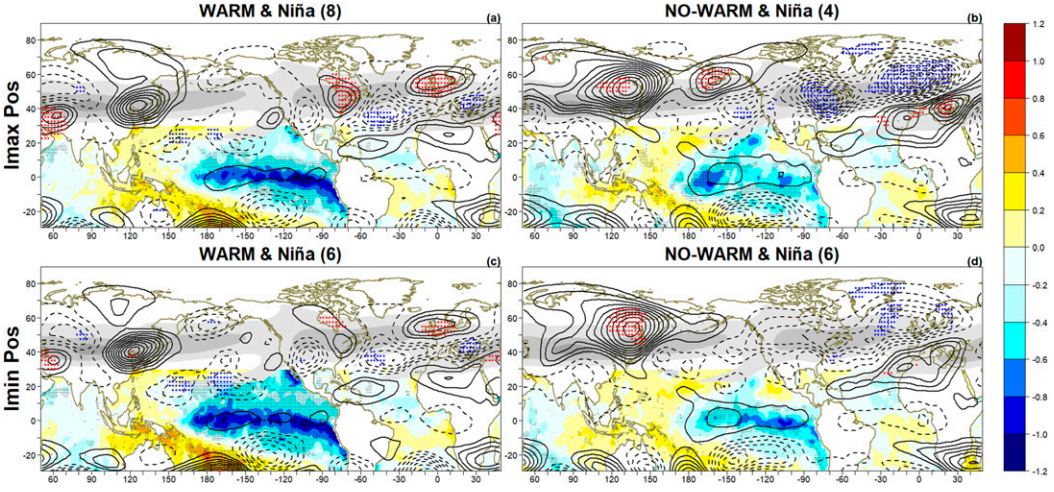

FIG. 7. Analysis of the teleconnection mechanism: ENSO teleconnections in JAS period 1953–75 SST (shaded) and Z200 (contours) anomalous composites for years with negative Niño-3.4 index. Columns show (a),(c) the years in which Imax and Imin present positive extremes and (b),(d) the years in which Imax and Imin do not present extremes. Cases are selected with standardized anomalies below −0.5 or above 0.5 std. The dotted regions indicate statistically significant areas, according to a *t* test at the 90% confidence level [black dots for SST; red (blue) dots for positive (negative) Z200]. Climatological U200 is plotted in gray (values between 10 and 60 m s^{-1}; interval: 10 m s^{-1}).

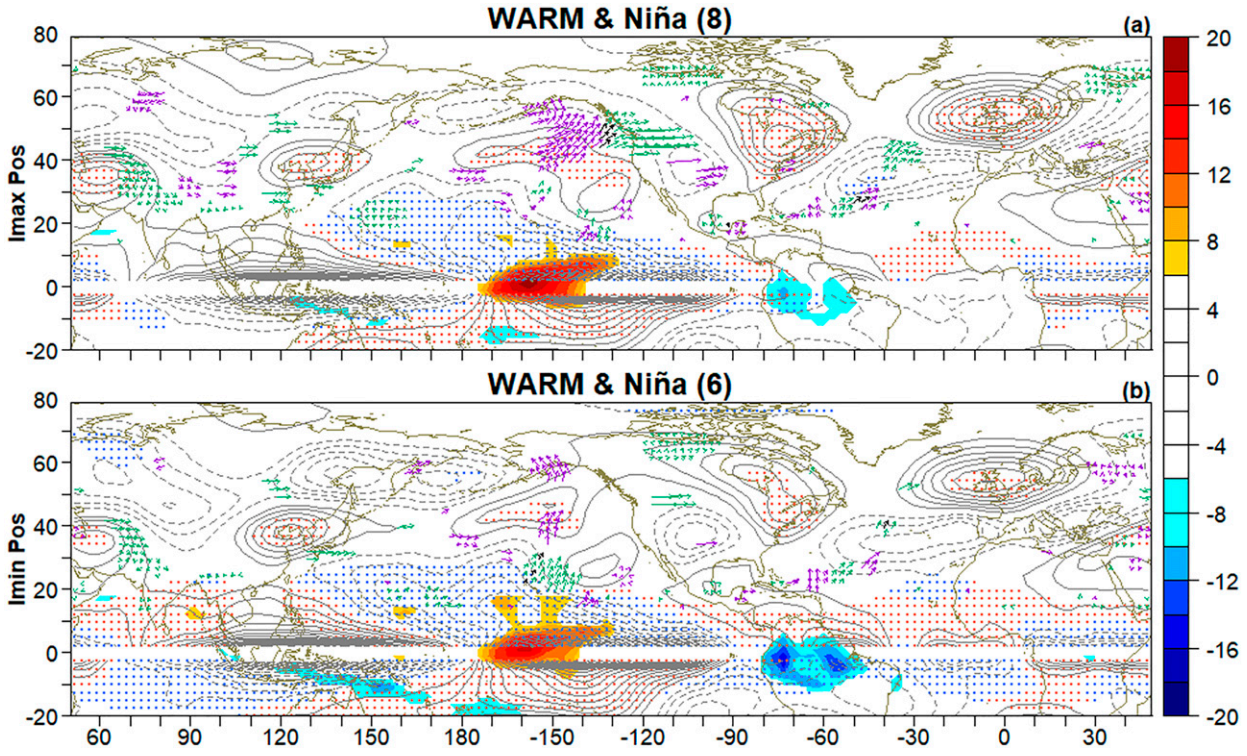

FIG. 8. OLR (W m^{-2}), streamfunction (contours; m^2 s^{-1}), and WAF (arrows; m^2 s^{-2}) at 200 hPa in the JAS period 1953–75 for WARM and Niña cases. The years are shown in which (a) Imax and (b) Imin present positive extremes and that match with the years with the negative extreme Niño-3.4 index. The dotted regions indicate statistically significant areas according to a Monte Carlo test at 90% confidence level [red (blue) dots for positive (negative) streamfunction]. Only the statistically significant values between 15° and 70°N of WAF are shown, according to a Monte Carlo test at the 90% confidence level. Violet and green arrows indicate zonally and meridionally significant areas, respectively; black arrows indicate that both aspects are statistically significant. Arrows scaled by 2. OLR is shown only between 20°S and 20°N.

atmospheric Rossby waves associated with the ENSO–WE teleconnection.

The different atmospheric patterns over WE could be explained by 1) a distinct oceanic forcing and/or 2) a different propagation of the teleconnection. The former is suggested by the anomalous SST configuration in Fig. 7, with stronger SST anomalies for LN episodes impacting temperatures (Figs. 7a,c) than those related to LN episodes with no impact on WE (Figs. 7b,d). In the cases with impact on WE, SST anomalies are strong (~−1°C) and reach the easternmost area of the equatorial Pacific, suggesting that well-developed LN events in summer, with sufficiently strong negative anomalies, are able to trigger a mechanism that reaches WE and impacts on WARM temperatures. Regarding the propagation mechanism, the teleconnection pattern for those LN events with no impact on WARM temperatures (Figs. 7b,d) is opposite to those impacting positive temperatures (Figs. 7a,c). In particular, the resulting positive center of geopotential anomalies over the North Sea associated with LN years impacting WARM events (Figs. 7a,c) is negative for the other LN episodes (Figs. 7b,d). This negative center over the North Sea is consistent with negative anomalies found in T850 (Figs. 5d,h).

The regional atmospheric structure associated with the WARM events (Figs. 7a,c) resembles the pattern usually associated with blocking events in the atmospheric west–east circulation over Europe (Barriopedro et al. 2006). Advective processes could explain the warmer conditions in the selected region, located at the south of that positive and blocking center, a feature that is absent for the remaining LNs.

Analysis of the large-scale teleconnection mechanism linking WARM events with LN episodes shows two anomalous cyclones straggling the equator, located at the northwest and at the southwest of the SST forcing (Figs. 7a,c). This structure resembles the atmospheric response to an equatorial diabatic cooling (Gill 1980). The resulting wave activity describes an arching-like structure from the central equatorial Pacific to North America (negative center over Hawaii and positive over California), where it seems to merge with a wavenumber-5 configuration trapped in the northern jet stream (gray shaded). The latter is consistent with the so-called CGT structure (Branstator 2002) and is in agreement with typical atmospheric responses identified in summer (DW05): positive anomaly centers at the North Sea, West Asia, East Asia, the northeastern Pacific, and Hudson Bay. The streamfunction and the WAF at 200 hPa are consistent with the proposed propagating mechanisms (Fig. 8): a CGT pattern at the midlatitudes together with an arching pattern triggered from the central Pacific. Moreover, the OLR (Fig. 8) indicates the region in

which the wave emerges, which is consistent with the propagation mechanism.

Furthermore, we analyze the evolution of the underlying LN events and find a clear growing tendency: LN reaches its peak in the following winter (Fig. 9; see also Fig. S4). In particular, therefore, developing LNs impact on WE temperatures in summer through a teleconnection pattern in which the CGT structure seems to be the dominant one, which is in agreement with D11.

The aforementioned result reinforces the robustness of the teleconnection between LN episodes and Tmax/Tmin, in summer, for the analyzed period (1953–75) and enables us to propose the following general hypotheses:

- Canonical LN impacts on positive WE temperature increasing its value.
- LN events impacting on summer temperature are in their growing phase.
- The teleconnection mechanism appears to begin with an arching-like pattern triggered from the central Pacific, which is trapped by the northern jet stream at midlatitudes where the CGT is activated.
- This teleconnection produces a positive anomaly center in WE, both in Z200 and T850.
- For EN events, no clear results are found.

Another important aspect that has not been addressed so far is the persistence of the SST anomalies over the tropical Pacific. This issue is relevant for predictability purposes. Analysis of the statistical significance of correlations between the EN-related anomalies in the previous seasons and the temperature response in WE enables us to form an idea of the potential predictability. This has been obtained for Niño-3.4 index in the selected period (1953–75; see Fig. 9); notice the linear nature of this analysis. However, as mentioned above, the teleconnection is biased to LN, so we draw conclusions only for this ENSO phase.

The negative correlations found at lag 0 (correlation between Imax/Imin and Niño-3.4 in JAS) agree with the results shown in Fig. 3. They cover from lag −4 until lag 8, reaching a peak around lag 2 and 4. Correlations change to positive values at lag −5 and remain positive for the whole previous natural year (from lag −5 to −18/20), with the positive peak (significant for Imin) around lag −12. Therefore, two consecutive ENSO peaks separated by 14–16 months are detected, which suggests a 2.5-yr ENSO cycle.

2) FALL (OND; 1990–2016)

Following the same methodology as in summer, we analyze the linearity of the WE response to ENSO with respect to the ENSO phase and flavor, and the related teleconnection mechanism.

We select a period (1990–2016) according to the positive correlations shown in Fig. 3. These correlations suggest positive (negative) extremes of temperature linked with positive (negative) extremes of ENSO (see also Fig. 10). For the COLD cases, there are 12 (13) events with lower anomalous values in Imax (Imin) (red and blue minus signs, respectively), but only in 2 (3) cases does a LN episode take place (among the total 7 LN events registered throughout this selected period; black dots vs green minus signs). All these findings suggest that LN is not a sufficient condition for triggering a COLD event, either for Tmax or for Tmin. These COLD cases should therefore be associated with other causes. For the WARM cases, higher values of Imax (Imin) are clearly related to EN. There are 9 (9) cases (red +/blue +), in which 6 (7) of them an EN event occurs (black dots); that is, almost 70% (90%) of the total. Furthermore, during this period 10 EN events were registered (green +), more than half of them matching with higher temperatures in WE (black dots). EN could therefore be a condition for triggering a WARM event.

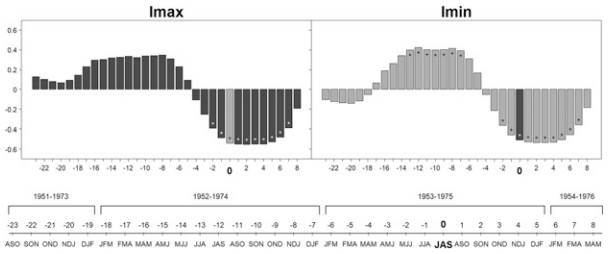

FIG. 9. Persistence of El Niño influence in JAS, showing a lag correlation between Imax/Imin and Niño-3.4 index (for the previous 23 and succeeding 8 three-month seasons) for the period 1953–75. (left) Correlations of Imax and Niño-3.4 index. The synchronous result (lag = 0) appears as the gray bar (0 on the x axis and in the legend). The leftmost bar shows the correlation between Imax and Niño-3.4 index in ASO of 20-yr window starting and ending 2 years before the selected period (1951–73, −23 on the x axis and in the legend). The rightmost bar indicates the correlation between Imax and Niño-3.4 index in MAM of 20-yr window starting and ending 1 year after the selected period (1954–76; 8 on the x axis and in the legend). The white points (black for lag = 0) indicate statistically significant correlations according to a t test at the 90% level. (right) As in the left panel, but for Imin. The lag = 0 is shown in black. The black points (white for lag = 0) indicate statistically significant correlations.

Over the NAES, cold conditions over the Atlantic and warm conditions over WE are identified at lower-tropospheric levels in relation to EN (Figs. 11b,f). However, unrelated EN episodes present a configuration characterized by a positive center over the west Atlantic and negative anomalies over WE (Figs. 11d,h), a pattern that cannot explain the occurrence of WARM temperatures in WE. The differences in EN characteristic and/or the teleconnection mechanism between those cases impacting on WARM temperatures and the others are analyzed in section 4.

It is also worth mentioning the intense positive anomalies around the Baltic Sea in the WARM cases not explained by EN (Figs. 11c,g). This region, which is outside our study area (WE), should be linked with internal variability or with another externally forced mechanism not associated with our proposed teleconnection.

For the WARM events, an intense (statistically significant for Imin) EN signal appears over the tropical Pacific (Figs. 12a,c). On the other hand, as expected, in the COLD cases, a very weak and nonsignificant LN signal emerges (Figs. 12b,d). The same analysis but for the first decades (1953–75) shows similar SST anomalies but noticeably weaker and nonsignificant (Fig. S5),

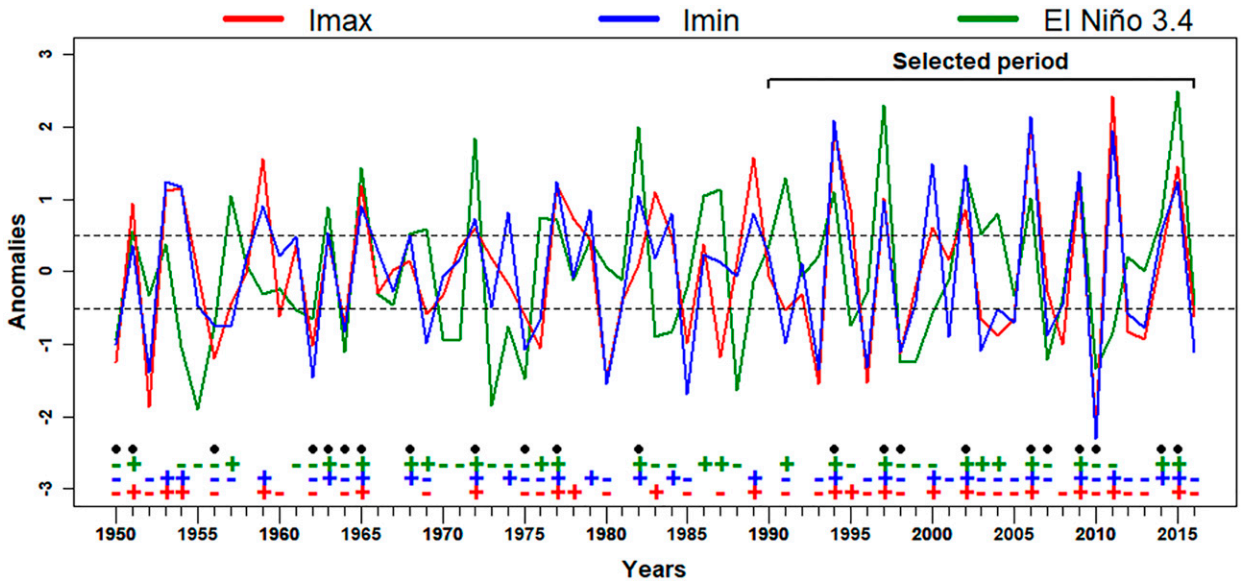

FIG. 10. OND standardized anomalies of Imax (red), Imin (blue), and Niño-3.4 (green) indices throughout the whole period (1950–2016). The horizontal black and dashed lines indicate thresholds (0.5 and −0.5 std). Years that exceed the positive threshold for Imax, Imin, and Niño-3.4 are indicated at the bottom with red, blue, and green plus signs (+), respectively. The years that exceed the negative threshold for Imax, Imin, and Niño-3.4 are indicated at the bottom with red, blue, and green minus signs (−), respectively. The black points represent the years that contribute to the positive correlation between Niño-3.4 and Imax and/or Imin (positive/negative Niño and positive/negative Imax or Imin).

which is consistent with the correlations obtained for this period (Fig. 3).

Henceforth, we focus on the EN–WARM temperatures teleconnection and, particularly, on the atmospheric pattern explaining it. We analyze and compare those EN events that have an impact on temperature (Figs. 13a,c) with those EN events with no impact on WE (Figs. 13b,d). As in summer, we find the way in which EN episodes with stronger SST anomalies are those impacting on WE. These EN events present anomalies that cover the whole equatorial Pacific, reaching values close to 2° (Figs. 13a,c). On the other hand, the remaining EN events, which have no impact on WE, present CP configuration with weaker amplitudes. The anomalous Z200 also indicates a wave structure that differs between EN events impacting WE temperature and those with no influence on WE (Figs. 13a,c vs Figs. 13b,d).

Focusing on the EN events impacting on WE (Figs. 13a,c), it appears that an arching-like wave structure is triggered from the central Pacific. At the northwest and the southwest of the maximum SST anomalies, two twin anticyclones appear straddling the equator, which resemble the typical Gill response (Gill 1980) to an equatorial diabatic heating. This baroclinic structure follows by an extratropical barotropic wave with a negative center located at California, a positive one at the east of North America, a negative center over the North Atlantic and a positive one reaching the western Mediterranean. The streamfunction (Fig. 14) is consistent with this structure. Furthermore, the related WAF (Fig. 14) shows significant interaction between the tropics and the extratropics. Two different Rossby wave sources are suggested over the tropical Pacific: one from the EP (~120°W) and the other from the CP (~150°–160 °W), the latter with a larger structure, which reaches higher latitudes. These two WAF intrusions produce distinct Rossby wavetrains, which can be partly attributed to the different interactions with the zonal mean flow, with the EP-related anomalies reaching the Atlantic branch of the jet stream and the CP-related anomalies reaching the North Pacific branch of the jet stream (see also the gray shaded areas in Fig. 13). Finally, the OLR shows negative anomalies linked with EN pattern, which is consistent with the area from which the wave emerges.

The resulting structure over the NAES agrees with the eastern Atlantic (EA) pattern in its positive phase (Barnston and Livezey 1987), which is reflected in strong positive anomalies center over WE, which (plus positive center found in T850 field in Fig. 11) explains conditions for higher stability and higher than usual surface temperature. This response agrees with King et al. (2017, 2018), who find a relationship in November between EN events and European warm temperatures (see Fig. 3a in King et al. 2018). However, in the present study we add new insights, since we determine the way in which this relation is not linear and is biased to EN events, but only for some particular periods.

Summarizing, our general hypotheses for ENSO teleconnection with temperatures in WE, in the selected period (1990–2016) and in the fall, are as follows:

- Canonical EN episodes impact on positive WE Tmax and Tmin, increasing their values.

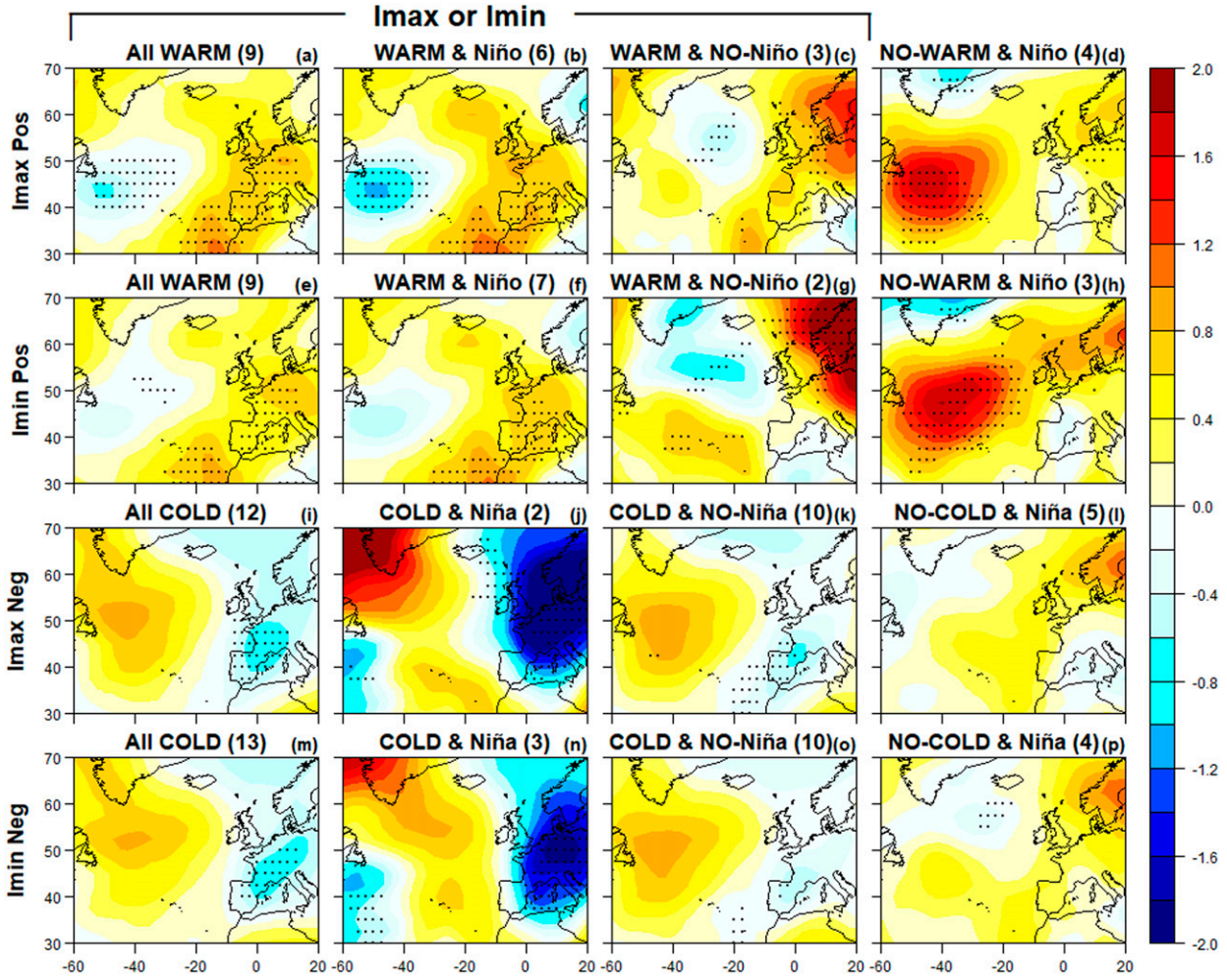

FIG. 11. Composites of T850 patterns and their relationship with ENSO in OND. Composites of anomalous temperature at 850 hPa calculated for years with extreme Imax or Imin and considering Niño-3.4 influence throughout the period 1990–2016 (selecting cases with standardized anomalies above 0.5 or below −0.5 std). Years corresponding with positive composites of (a) Imax and (e) Imin (WARM cases) are divided into years (b),(f) with positive Niño-3.4 index and (c),(g) with no El Niño. (d),(h) Also shown are composites for positive Niño-3.4 events that do not match with WARM cases. (i)–(p) As in (a)–(h), but for negative composites of (i) Imax and (m) Imin (COLD cases) and (j),(k),(n),(o) comparing with the negative composite of the Niño-3.4 index. (l),(p) Negative Niño-3.4 composites that do not match with the COLD cases. The dotted regions indicate statistically significant areas according to a *t* test at the 90% confidence level.

- The teleconnection mechanism seems to follow an arching-like pattern.
- The planetary Rossby waves are able to reach the NAES and generate an EA response, which in turn explains the impact on WE temperatures.
- For LN events, no clear results are found.

As for the summer season, we compute the correlation scores between Imax/Imin and Niño-3.4 at different time lags (Fig. 15) in order to assess possible predictability. It should be pointed out that, although this is a linear analysis, we should interpret Fig. 15 only for positive ENSO phases (EN). The results show positive and statistically significant correlations between the variables and Niño-3.4 at lag 0 and in the three to four previous/coming seasons (from lag −4 to lag 3). Hence, an EN event that begins in summer correlates with WARM temperatures of the next fall–winter period, when it reaches its peak. Before lag −4, the correlations become smaller and change to negative values. Between 8/9 and 17 preceding seasons (from lag −8/−9 to −17), negative and statistically significant correlations are found, which means that during approximately the previous natural year a LN event is detected. As in summer, ENSO cycle also seems to last around 2.5 years.

4. Summary and discussion

This study concerns the search for possible predictors of WE temperatures. We find that ENSO impacts in a nonlinear, nonstationary way on WE temperatures in summer and fall seasons. This correlation is investigated using high-quality data

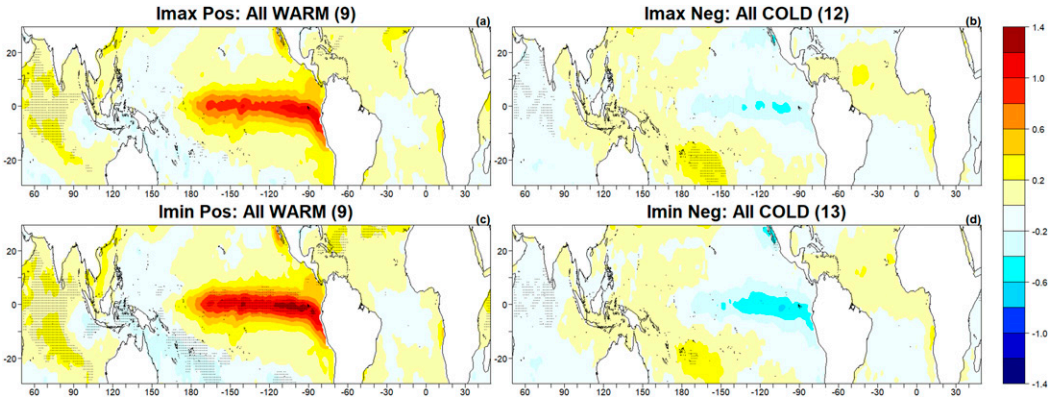

FIG. 12. Anomalies around the equator in OND: SST anomalous composites for years with positive and negative extreme of (a),(b) Imax and (c),(d) Imin throughout the period 1990–2016 (selecting cases with standardized anomalies (a),(c) above 0.5 std and (b),(d) below −0.5 std). The dotted regions indicate statistically significant areas according to a *t* test at the 90% confidence level.

of Tmax and Tmin in a certain region within WE, which is the area of maximum variability on the European continent.

Statistically significant correlation scores are obtained for decades before the 1980s. These correlations are found to be negative in summer (JAS). From the 1980s onward, the link changes and positive correlations are obtained. Indeed, for the decades after the 1980s, the strongest influence of ENSO on WE temperatures appears in fall (OND). This propagation structure identified in the correlation analysis between summer and fall was already suggested in previous studies (LP12) and point to a change in the seasonal evolution of the ENSO impact on WE.

The results also indicate a nonlinear response to ENSO, in such a way that the influence is found only for warmer atmospheric conditions, LN being the phase with this impact in JAS and EN phase in OND.

Before the 1980s, an anticyclonic blocking pattern is found for the local summer atmospheric response to LN, in agreement with blocking structures associated with summer heat waves over WE (Cassou et al. 2005). In the case of EN, a similar association is identified in fall season for decades after the 1990s. As shown in Fig. 16a, the climatological conditions over the tropical oceans are colder (warmer) for the 1950s to the 1980s (the 1990s to the 2010s), which may affect the propagation of atmospheric Rossby waves and the available potential energy released by convection from the tropics (Johnson and Xie 2010, and references therein). However, the nonstationary

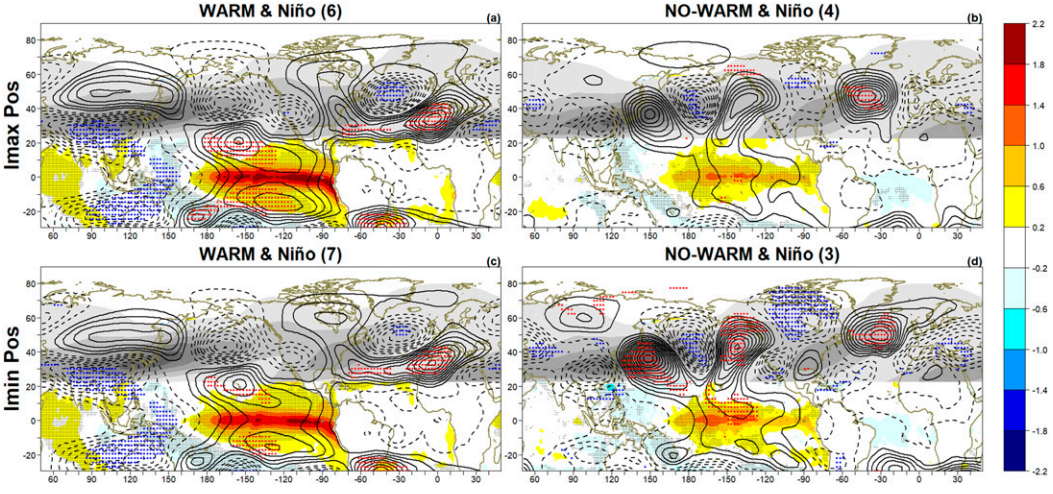

FIG. 13. Analysis of the teleconnection mechanism: ENSO teleconnections in OND period 1990–2016 SST (shaded) and Z200 (contours) anomalous composites for years with positive Niño-3.4 index. Columns show (a),(c) the years in which Imax and Imin present positive extremes and (b),(d) the years in which Imax and Imin do not present extremes. Cases are selected with standardized anomalies below −0.5 std or above 0.5 std. The dotted regions indicate statistically significant areas according to a *t* test at the 90% confidence level [black dots for SST; red (blue) dots for positive (negative) Z200]. Climatological U200 is plotted in gray (values between 10 and 60 m s^{-1}; interval: 10 m s^{-1}).

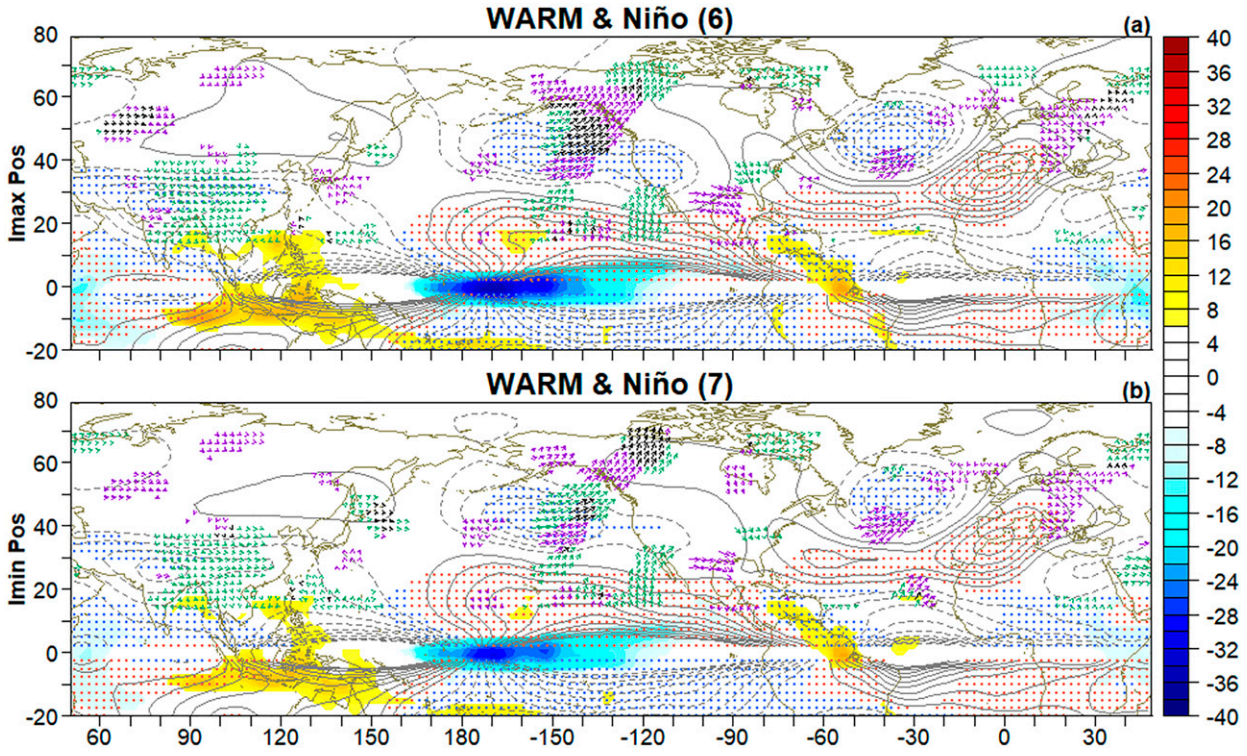

FIG. 14. OLR ($W\,m^{-2}$), streamfunction (contours; $m^2\,s^{-1}$), and WAF (arrows; $m^2\,s^{-2}$) at 200 hPa in the OND period 1990–2016 for WARM and Niño cases, showing the years in which (a) Imax and (b) Imin present positive extremes and that match with the years with the positive extreme Niño-3.4 index. The dotted regions indicate statistically significant areas according to a Monte Carlo test at the 90% confidence level [red (blue) dots for positive (negative) streamfunction]. Only the statistically significant values between 15° and 70°N of WAF are shown, according to a Monte Carlo test at the 90% confidence level. Violet and green arrows indicate zonally and meridionally significant areas, respectively; black arrows indicate that both aspects are statistically significant. Arrows scaled by 0.5. OLR is shown only between 20°S and 20°N.

ENSO teleconnection with Europe is still under debate. Some authors point to the Atlantic Ocean as a modulator of some teleconnection pathways (e.g., Sutton and Hodson 2003), while others find that the base state of both the Atlantic and Pacific Oceans plays an important role in this nonstationary link (e.g., LP15, LP16). Finally, other authors attribute this changing impact to global warming (e.g., Vecchi and Soden 2007). Recent research shows that global warming is linked to the amplification of Rossby waves and the CGT in summer (Teng and Branstator 2019), and Kornhuber et al. (2020) found a relation between this amplification and stronger heatwaves around the world. Nevertheless, the results presented here also point to natural variability modes as potential modulators of the ENSO teleconnection with WE. For instance, the link identified here between LN events and Tmax/Tmin over WE in summer occurs in those decades before the 1980s in coincidence with a negative phase of the interdecadal Pacific oscillation (IPO; Salinger et al. 2001). Thus, the negative anomalies associated with LN, together with the cold background conditions related to the negative IPO, may provide the necessary condition for triggering an atmospheric teleconnection to Europe. On the other hand, after the 1990s, our results indicate a transition (from summer to fall) of the season in which ENSO influences WE temperatures, although in this case the link occurs in association with EN episodes. While other factors may also be influencing this, the emergence of this EN teleconnection with WE in the 1990s is consistent with 1) the positive IPO phase taking place during that period and 2) the related increase of frequency in EN episodes. Nevertheless, no conclusive reason sustains the propagation of the impact from summer to fall. At this point, further analysis will be needed in order to clarify whether these changes represent a real displacement of the season in which ENSO impact occurs or if they reflect an intermittent nature of this teleconnection in each season.

To better understand the teleconnection differences among decades, additional factors that should be also taken into account are the characteristics of the climatological northern jet stream (Figs. 16b–d). Zonal wind anomalies at upper troposphere are mostly positive at midlatitudes (40°–60°N) and negative at the subtropics (20°–40°N), with the exception of the longitudes between 60° and 160°E (Fig. 16b). The resultant anomalous configuration indicates a northward shift of the jet in the recent decades. In that decades, a significant warming appears over the tropical belt in such a way that a marked meridional gradient emerges. The latter seems to be behind the northward displacement of the zonal jet. This shift is clearer over the Atlantic sector (Fig. 16b) and could be playing an

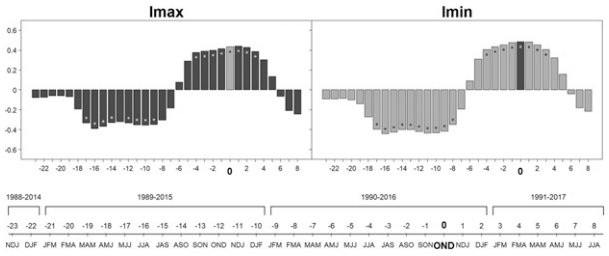

FIG. 15. Persistence of El Niño influence in OND. Lag correlation between Imax/Imin and the Niño-3.4 index (for the previous 23 and succeeding 8 three-month seasons) for the period 1990–2016. (left) Correlations of Imax and Niño-3.4 index. The synchronous result (lag = 0) appears as the gray bar (0 on the *x* axis and in the legend). The leftmost bar shows the correlation between Imax and Niño-3.4 index in NDJ of a 20-yr window starting and ending 2 years before the selected period (1988–2014, −23 on the *x* axis and in the legend). The rightmost bar indicates the correlation between Imax and Niño-3.4 index in JJA of a 20-yr window starting and ending 1 year after the selected period (1991–2017; 8 on the *x* axis and in the legend). The white points (black for lag = 0) indicate statistically significant correlations according to a *t* test at the 90% level. (right) As in the left panel, but for Imin. The lag = 0 is shown in black. The black points (white for lag = 0) indicate statistically significant correlations.

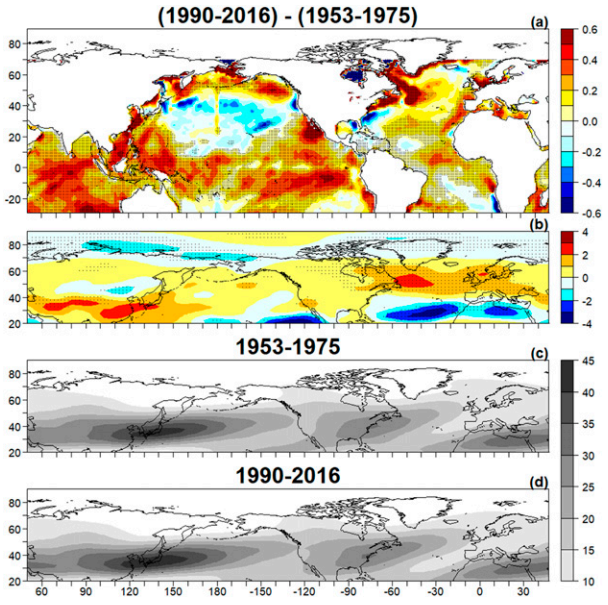

FIG. 16. Changes in the climatological background conditions. (a) Difference between the 1990–2016 and 1953–75 SST annual means. (b) As in (a), but for U200. (c) Climatological U200 for 1953–75. (d) As in (c), but for 1990–2016. The dotted regions indicate statistically significant areas according to a *t* test at the 90% confidence level. For SST, the climate signal has been removed.

important role in our changing teleconnection as explained next. Following the seasonal cycle, the jet stream is placed northward in boreal summer compared to winter (Branstator and Teng 2017). This fact, together with the decadal shift of the jet, has an impact on the role of the jet in the teleconnections along the seasons. In summer, a more zonal jet is acting as a wave train for a CGT, reaching northern areas in the second period (1990–2016), out of our study region (Fig. S6). On the contrary, during the second period but in fall, the jet stream presents a weakening on the eastern flank of the subtropical North Pacific (Fig. S7), favoring an arching-like wave configuration reaching our study region. This changing position of the jet stream may be, in turn, due to the natural variability of ocean SST (LP15) and/or the anthropogenic forcing (Woollings and Blackburn 2012). Indeed, Lin et al. (2016) found that SST anomalies linked with the AMV play an important role in the CGT pattern, which is trapped in the jet, in summer.

In the future, further research should be therefore conducted in order to better understand the role of both global warming and decadal variability in the modulation of the tropical–extratropical teleconnections, and, if possible, to integrate this information into the current seasonal prediction systems. To this aim, sensitivity experiments with different background conditions and ENSO flavors and phases should be conducted.

It is also interesting to note the fact that previous studies concerning the influence of ENSO on the European climate have paid little attention to the summer season, for which the signature of ENSO has been described as marginal (Shaman 2014b). In our opinion, the principal reasons that account for this apparent contradiction with our analysis are 1) the variable considered (temperature and not rainfall) and 2) the time period analyzed. In this sense, Shaman (2014b) investigates the impact of ENSO on European precipitation during a period (1950–2013) similar to our whole period (1950–2016). In the present study, however, we seek windows of opportunity; that is, decades in which the influence of ENSO on WE temperature is significant during a 20-yr period (LP12). We therefore propose that while the ENSO–WE teleconnection in summer does exist, it does not have the same impact on rainfall as on temperature; being nonstationary but significant and robust for temperature (Tmax and Tmin), but weak and marginal for precipitation.

The underlying mechanism in summer for decades before the 1980s is associated with a wave pattern triggered from the central Pacific and trapped by the jet stream, thereby producing a wavenumber-5 CGT structure (Branstator 2002; DW05; Wang et al. 2012). For those weaker LNs with no impact on WE temperatures, the wave triggered from the equatorial Pacific is unable to reach the jet stream and modulate the global circulation (the WAF and the streamfunction are shown in Fig. S8).

Moreover, D11 described the differences between ENSO teleconnection in summers when the event is developing and when it is decaying. These authors found a CGT-like pattern for the years when ENSO is developing. Analysis of the evolution of our LN events also reveal a growing pattern (Fig. S5), which brings our results into agreement with D11.

No clear results are found for EN events, perhaps because of the limited number of years detected in the period analyzed. Only four EN cases are identified over 23 years (1953–75), a period coinciding with a negative phase of IPO (Salinger et al. 2001). In this period, 9 (6) cases with colder Imax (Imin) than

usual are found, fewer than half of which are related to EN episodes (4 and 2, respectively). Thus, most of the cases with colder temperatures seem to be related with local processes or internal variability (linked perhaps with dominant modes in the study region such as the NAO). Even so, all EN events impact WE Tmax and the underlying teleconnection mechanism seems to be very similar to that found for LN cases (Figs. S2 and S3). This result points to the negative IPO phase as the major explanation for the fact that our teleconnection with WE is biased to LN events (and absent for EN events).

For decades after the 1990s, however, the underlying mechanisms in fall season are related to an arching-like pattern triggered from the central equatorial Pacific, crossing the United States, and reaching WE. The resultant pattern resembles an EA positive-phase configuration (King et al. 2017, 2018). The arching pattern found does not totally agree with either the TNH or the PNA, patterns that are usually linked with ENSO. Nevertheless, a positive anomalous tongue crossing the Atlantic and reaching WE is found, a structure similar (shifted northward) to the PNA-like teleconnection pattern described by Yu et al. (2015) in winter.

For weaker and CP-like ENs with no impact on WE temperatures, the SST anomalies do not seem to constitute an energy source capable of triggering a wave that modulates the global circulation (Figs. 13b,d). The typical Gill response is absent, and the midlatitude zonal structure does not appear to be affected by ENSO. The WAF and the streamfunction confirms this hypothesis; there is no intrusion of wave activity from subtropics to the extratropics and the streamfunction does not present significant anomalies in the tropics (Fig. S9).

Thus, an important outcome of our study is that only anomalous warm conditions in WE (i.e., Tmin and Tmax higher than usual) seem to be predictable from ENSO. However, this occurs for certain periods and by means of distinct dynamical mechanisms, associated with LN events in summer during the 1953–75 period and with EN events in fall for the 1990–2016 period. Unfortunately, due to the changing impact found between decades and the resulting limited number of years for each analysis, the sampling is (sometimes) small. Thus, further research with sensitivity experiments will be useful to increase the robustness of our findings.

Finally, our results also shed light on the role played by the ENSO cycle in the above-mentioned influence over WE temperature. In summer, warmer than usual temperatures linked to LN appear when the event in the Pacific is developing and the peak is reached in the following winter. This LN event (in progress during summertime) is preceded by an EN event in such a way that an EN-to-LN transition is found (Fig. 9). In fall, the EN events impacting on warmer than usual temperatures in WE are at their peak and come from a LN event in the previous fall and winter (Fig. 15). These transitions in summer and fall are both statistically significant and suggests a 2.5-yr ENSO cycle. This result may increase the predictive capability of the European climate from the ENSO-related SSTs, and emerges as an important contribution of the present study, particularly for summer, a season with very limited predictive skill (Ghosh et al. 2017). This and other related aspects should be analyzed further in future studies.

Acknowledgments. This research has been partially supported by the Spanish PRE4CAST project (Ref. CGL2017:86415-R). We acknowledge the E-OBS dataset from the EU-FP6 project ENSEMBLES (http://ensembles-eu.metoffice.com) and the data providers in the ECA&D project (http://www.ecad.eu). All the calculations and plots were carried out using the R programming language (R Core Team 2020). Finally, we thank the anonymous reviewers for their suggestions which have contributed to improve the manuscript.

REFERENCES

Ayarzagüena, B., S. Ineson, N. J. Dunstone, M. P. Baldwin, and A. A. Scaife, 2018a: Intraseasonal effects of El Niño–Southern Oscillation on North Atlantic climate. *J. Climate*, **31**, 8861–8873, https://doi.org/10.1175/JCLI-D-18-0097.1.

——, J. López-Parages, M. Iza, N. Calvo, and B. Rodríguez-Fonseca, 2018b: Stratospheric role in interdecadal changes of El Niño impacts over Europe. *Climate Dyn.*, **52**, 1173–1186, https://doi.org/10.1007/s00382-018-4186-3.

Bador, M., L. Terray, J. Boé, S. Somot, A. Alias, A. L. Gibelin, and B. Dubuisson, 2017: Future summer mega-heatwave and record-breaking temperatures in a warmer France climate. *Environ. Res. Lett.*, **12**, 074025, https://doi.org/10.1088/1748-9326/aa751c.

Ballester, J., X. Rodó, and F. Giorgi, 2010: Future changes in Central Europe heat waves expected to mostly follow summer mean warming. *Climate Dyn.*, **35**, 1191–1205, https://doi.org/10.1007/s00382-009-0641-5.

Barnston, A. G., and R. E. Livezey, 1987: Classification, seasonality and persistence of low-frequency atmospheric circulation patterns. *Mon. Wea. Rev.*, **115**, 1083–1126, https://doi.org/10.1175/1520-0493(1987)115<1083:CSAPOL>2.0.CO;2.

——, ——, and M. S. Halpert, 1991: Modulation of Southern Oscillation–Northern Hemisphere mid-winter climate relationships by the QBO. *J. Climate*, **4**, 203–217, https://doi.org/10.1175/1520-0442(1991)004<0203:MOSONH>2.0.CO;2.

Barriopedro, D., R. García-Herrera, A. R. Lupo, and E. Hernández, 2006: A climatology of Northern Hemisphere blocking. *J. Climate*, **19**, 1042–1063, https://doi.org/10.1175/JCLI3678.1.

——, E. M. Fischer, J. Luterbacher, R. M. Trigo, and R. García-Herrera, 2011: The hot summer of 2010: Redrawing the temperature record map of Europe. *Science*, **332**, 220–224, https://doi.org/10.1126/science.1201224.

Bell, C. J., L. J. Gray, A. J. Charlton-Perez, M. M. Joshi, and A. A. Scaife, 2009: Stratospheric communication of El Niño teleconnections to European winter. *J. Climate*, **22**, 4083–4096, https://doi.org/10.1175/2009JCLI2717.1.

Bergman, K. H., 1984: The climate of autumn 1983—Featuring the conclusion of a major El Niño event. *Mon. Wea. Rev.*, **112**, 1441–1456, https://doi.org/10.1175/1520-0493(1984)112<1441:TCOATC>2.0.CO;2.

Bladé, I., M. Newman, M. A. Alexander, and J. D. Scott, 2008: The late fall extratropical response to ENSO: Sensitivity to coupling and convection in the tropical west Pacific. *J. Climate*, **21**, 6101–6118, https://doi.org/10.1175/2008JCLI1612.1.

Bonsal, B., and A. Shabbar, 2011: Large-scale climate oscillations influencing Canada, 1900–2008. Canadian Biodiversity: Ecosystem Status and Trends 2010, Tech. Thematic Rep. 4, Canadian Councils of Resource Ministers, 15 pp.

Bracco, A., F. Kucharski, R. Kallummal, and F. Molteni, 2004: Internal variability, external forcing and climate trends in multi-decadal AGCM ensembles. *Climate Dyn.*, **23**, 659–678, https://doi.org/10.1007/s00382-004-0465-2.

Brands, S., 2017: Which ENSO teleconnections are robust to internal atmospheric variability? *Geophys. Res. Lett.*, **44**, 1483–1493, https://doi.org/10.1002/2016GL071529.

Branstator, G., 2002: Circumglobal teleconnections, the jet stream waveguide, and the North Atlantic Oscillation. *J. Climate*, **15**, 1893–1910, https://doi.org/10.1175/1520-0442(2002)015<1893:CTTJSW>2.0.CO;2.

——, and F. Selten, 2009: "Mode of variability" and climate change. *J. Climate*, **22**, 2639–2658, https://doi.org/10.1175/2008JCLI2517.1.

——, and H. Teng, 2017: Tropospheric waveguide teleconnections and their seasonality. *J. Atmos. Sci.*, **74**, 1513–1532, https://doi.org/10.1175/JAS-D-16-0305.1.

Brönnimann, S., 2007: Impact of El Niño–Southern Oscillation on European climate. *Rev. Geophys.*, **45**, RG3003, https://doi.org/10.1029/2006RG000199.

Bulić, I. H., and F. Kucharski, 2012: Delayed ENSO impact on spring precipitation over North/Atlantic European region. *Climate Dyn.*, **38**, 2593–2612, https://doi.org/10.1007/s00382-011-1151-9.

——, B. Mezzina, F. Kucharski, P. Ruggieri, and M. P. King, 2017: Wintertime ENSO influence on late spring European climate: The stratospheric response and the role of North Atlantic SST. *Int. J. Climatol.*, **37**, 87–108, https://doi.org/10.1002/joc.4980.

Cagnazzo, C., and E. Manzini, 2009: Impact of the stratosphere on the winter tropospheric teleconnections between ENSO and the North Atlantic and European region. *J. Climate*, **22**, 1223–1238, https://doi.org/10.1175/2008JCLI2549.1.

Cassou, C., L. Terray, and A. S. Phillips, 2005: Tropical Atlantic influence on European heat waves. *J. Climate*, **18**, 2805–2811, https://doi.org/10.1175/JCLI3506.1.

Chen, T. C., 2002: A north Pacific short-wave train during the extreme phases of ENSO. *J. Climate*, **15**, 2359–2376, https://doi.org/10.1175/1520-0442(2002)015<2359:ANPSWT>2.0.CO;2.

Cornes, R. C., G. van der Schrier, E. J. M. van den Besselaar, and P. D. Jones, 2018: An ensemble version of the E-OBS temperature and precipitation data sets. *J. Geophys. Res.*, **123**, 9391–9409, https://doi.org/10.1029/2017JD028200.

De Bono, A., G. Giuliani, S. Kluster, and P. Peduzzi, 2004: Impacts of summer 2003 heat wave in Europe. Environment Alert Bulletin 2, UNEP, 4 pp.

Della-Marta, P. M., J. Luterbacher, H. von Weissenfluh, E. Xoplaki, M. Brunet, and H. Wanner, 2007: Summer heat waves over western Europe 1880–2003, their relationship to large-scale forcings and predictability. *Climate Dyn.*, **29**, 251–275, https://doi.org/10.1007/s00382-007-0233-1.

Deser, C., and A. S. Phillips, 2009: Atmospheric circulation trends, 1950–2000: The relative roles of sea surface temperature forcing and direct atmospheric radiative forcing. *J. Climate*, **22**, 396–413, https://doi.org/10.1175/2008JCLI2453.1.

——, I. R. Simpson, K. A. McKinnon, and A. S. Phillips, 2017: The Northern Hemisphere extratropical atmospheric circulation response to ENSO: How well do we know it and how do we evaluate models accordingly? *J. Climate*, **30**, 5059–5082, https://doi.org/10.1175/JCLI-D-16-0844.1.

Ding, Q., and B. Wang, 2005: Circumglobal teleconnection in the Northern Hemisphere summer. *J. Climate*, **18**, 3483–3505, https://doi.org/10.1175/JCLI3473.1.

——, ——, J. M. Wallace, and G. Branstator, 2011: Tropical–extratropical teleconnections in boreal summer: Observed interannual variability. *J. Climate*, **24**, 1878–1896, https://doi.org/10.1175/2011JCLI3621.1.

Ebbesmeyer, C. C., D. R. Cayan, D. R. McLain, F. H. Nichols, D. H. Peterson, and K. T. Redmond, 1991: 1976 step in the Pacific climate: Forty environmental changes between 1968–1975 and 1977–1984. *Proc. Seventh Annual Pacific Climate Workshop*, Pacific Grove, CA, 115–126, http://aquaticcommons.org/4562/.

Fischer, K., M. Klockmann, and E. Reim, 2014: Strong negative effects of simulated heat waves in a tropical butterfly. *J. Exp. Biol.*, **217**, 2892–2898, https://doi.org/10.1242/jeb.106245.

Frauen, C., D. Dommenget, N. Tyrrell, M. Rezny, and S. Wales, 2014: Analysis of the nonlinearity of El Niño–Southern Oscillation teleconnections. *J. Climate*, **27**, 6225–6244, https://doi.org/10.1175/JCLI-D-13-00757.1.

García-Herrera, R., J. Díaz, R. M. Trigo, J. Luterbacher, and E. M. Fischer, 2010: A review of the European summer heat wave of 2003. *Crit. Rev. Environ. Sci. Technol.*, **40**, 267–306, https://doi.org/10.1080/10643380802238137.

García-Serrano, J., B. Rodríguez-Fonseca, I. Bladé, P. Zurita-Gotor, and A. de la Cámara, 2011: Rotational atmospheric circulation during North Atlantic–European winter: The influence of ENSO. *Climate Dyn.*, **37**, 1727–1743, https://doi.org/10.1007/s00382-010-0968-y.

Ghosh, R., W. A. Müller, J. Baehr, and J. Bader, 2017: Impact of observed North Atlantic multidecadal variations to European summer climate: A linear baroclinic response to surface heating. *Climate Dyn.*, **48**, 3547–3563, https://doi.org/10.1007/s00382-016-3283-4.

Gill, A. E., 1980: Some simple solutions for heat induced tropical circulation. *Quart. J. Roy. Meteor. Soc.*, **106**, 447–462, https://doi.org/10.1002/qj.49710644905.

Giorgi, F., 2006: Climate change hot-spots. *Geophys. Res. Lett.*, **33**, L08707, https://doi.org/10.1029/2006GL025734.

Guerreiro, S. B., R. J. Dawson, C. Kilsby, E. Lewis, and A. Ford, 2018: Future heat-waves, droughts and floods in 571 European cities. *Environ. Res. Lett.*, **13**, 034009, https://doi.org/10.1088/1748-9326/aaaad3.

Hoerling, M. P., J. W. Hurrell, and T. Xu, 2001: Tropical origins for recent North Atlantic climate change. *Science*, **292**, 90–92, https://doi.org/10.1126/science.1058582.

——, ——, ——, G. T. Bates, and A. S. Phillips, 2004: Twentieth century North Atlantic climate change. Part II: Understanding the effect of Indian Ocean warming. *Climate Dyn.*, **23**, 391–405, https://doi.org/10.1007/s00382-004-0433-x.

Hurrell, J. W., and C. Deser, 2009: North Atlantic climate variability: The role of the North Atlantic Oscillation. *J. Mar. Syst.*, **78**, 28–41, https://doi.org/10.1016/j.jmarsys.2008.11.026.

——, M. P. Hoerling, A. S. Phillips, and T. Xu, 2004: Twentieth century North Atlantic climate change. Part I: Assessing determinism. *Climate Dyn.*, **23**, 371–389, https://doi.org/10.1007/s00382-004-0432-y.

Ineson, S., and A. A. Scaife, 2009: The role of the stratosphere in the European climate response to El Niño. *Nat. Geosci.*, **2**, 32–36, https://doi.org/10.1038/ngeo381.

IPCC, 2014: Summary for policymakers. *Climate Change 2014: Synthesis Report*, IPCC, 1–32, https://www.ipcc.ch/report/ar5/syr/.

Johnson, N. C., and S.-P. Xie, 2010: Changes in the sea surface temperature threshold for tropical convection. *Nat. Geosci.*, **3**, 842–845, https://doi.org/10.1038/ngeo1008.

Kalnay, E., and Coauthors, 1996: The NCEP/NCAR 40-Year Reanalysis Project. *Bull. Amer. Meteor. Soc.*, **77**, 437–471, https://doi.org/10.1175/1520-0477(1996)077<0437:TNYRP>2.0.CO;2.

Kiladis, G. N., and H. F. Diaz, 1989: Global climatic anomalies associated with extremes in the Southern Oscillation. *J. Climate*, **2**, 1069–1090, https://doi.org/10.1175/1520-0442(1989)002<1069:GCAAWE>2.0.CO;2.

King, M. P., I. Herceg-Bulić, F. Kucharski, and N. Keenlyside, 2017: Interannual tropical Pacific sea surface temperature anomalies teleconnection to Northern Hemisphere atmosphere in November. *Climate Dyn.*, **50**, 1881–1899, https://doi.org/10.1007/s00382-017-3727-5.

——, ——, I. Bladé, J. García-Serrano, N. Keenlyside, F. Kucharski, C. Li, and S. Sobolowski, 2018: Importance of late fall ENSO teleconnection in the Euro-Atlantic sector. *Bull. Amer. Meteor. Soc.*, **99**, 1337–1343, https://doi.org/10.1175/BAMS-D-17-0020.1.

Knight, J. R., C. K. Folland, and A. A. Scaife, 2006: Climate impacts of the Atlantic multidecadal oscillation. *Geophys. Res. Lett.*, **33**, L17706, https://doi.org/10.1029/2006GL026242.

Kornhuber, K., D. Coumou, E. Vogel, C. Lesk, J. F. Donges, J. Lehmann, and R. M. Horton, 2020: Amplified Rossby waves enhance risk of concurrent heatwaves in major breadbasket regions. *Nat. Climate Change*, **10**, 48–53, https://doi.org/10.1038/s41558-019-0637-z.

Kyselý, J., 2010: Recent severe heat waves in central Europe: How to view them in a long-term prospect? *Int. J. Climatol.*, **30**, 89–109, https://doi.org/10.1002/joc.1874.

Lau, K.-M., and L. Peno, 1992: Dynamics of atmospheric teleconnections during the northern summer. *J. Climate*, **5**, 140–158, https://doi.org/10.1175/1520-0442(1992)005<0140:DOATDT>2.0.CO;2.

Lin, J.-S., B. Wu, and T.-J. Zhou, 2016: Is the interdecadal circumglobal teleconnection pattern excited by the Atlantic multidecadal oscillation? *Atmos. Oceanic Sci. Lett.*, **9**, 451–457, https://doi.org/10.1080/16742834.2016.1233800.

López-Parages, J., and B. Rodríguez-Fonseca, 2012: Multidecadal modulation of El Niño influence on the Euro-Mediterranean rainfall. *Geophys. Res. Lett.*, **39**, L02704, https://doi.org/10.1029/2011GL050049.

——, ——, and L. Terray, 2015: A mechanism for the multidecadal modulation of ENSO teleconnection with Europe. *Climate Dyn.*, **45**, 867–880, https://doi.org/10.1007/s00382-014-2319-x.

——, ——, D. Dommenget, and C. Frauen, 2016: ENSO influence on the North Atlantic European climate: A non-linear and non-stationary approach. *Climate Dyn.*, **47**, 2071–2084, https://doi.org/10.1007/s00382-015-2951-0.

Manzini, E., M. A. Giorgetta, M. Esch, L. Kornblueh, and E. Roeckner, 2006: The influence of sea surface temperatures on the northern winter stratosphere: Ensemble simulations with the MAECHAM5 model. *J. Climate*, **19**, 3863–3881, https://doi.org/10.1175/JCLI3826.1.

Mezzina, B., J. García-Serrano, I. Bladé, and F. Kucharski, 2020: Dynamics of the ENSO teleconnection and NAO variability in the North Atlantic–European late winter. *J. Climate*, **33**, 907–923, https://doi.org/10.1175/JCLI-D-19-0192.1.

Mo, K. C., and R. E. Livezey, 1986: Tropical–extratropical geopotential height teleconnections during the Northern Hemisphere winter. *Mon. Wea. Rev.*, **114**, 2488–2515, https://doi.org/10.1175/1520-0493(1986)114<2488:TEGHTD>2.0.CO;2.

Müller, W. A., and E. Roeckner, 2008: ENSO teleconnections in projections of future climate in ECHAM5/MPI-OM. *Climate Dyn.*, **31**, 533–549, https://doi.org/10.1007/s00382-007-0357-3.

Ossó, A., R. Sutton, L. Shaffrey, and B. Dong, 2018: Observational evidence of European summer weather patterns predictable from spring. *Proc. Natl. Acad. Sci. USA*, **115**, 59–63, https://doi.org/10.1073/pnas.1713146114.

Pozo-Vázquez, D., S. R. Gámiz-Fortis, J. Tovar-Pescador, M. J. Esteban-Parra, and Y. Castro-Díez, 2005: North Atlantic winter SLP anomalies based on the autumn ENSO state. *J. Climate*, **18**, 97–103, https://doi.org/10.1175/JCLI-3210.1.

Raible, C. C., U. Luksch, and K. Fraedrich, 2003: Precipitation and Northern Hemisphere regimes. *Atmos. Sci. Lett.*, **5**, 43–55, https://doi.org/10.1016/j.atmoscilet.2003.12.001.

Rayner, N. A., D. E. Parker, E. B. Horton, C. K. Folland, L. V. Alexander, and D. P. Rowell, 2003: Global analyses of sea surface temperature, sea ice, and night marine air temperature since the late nineteenth century. *J. Geophys. Res.*, **108**, 4407, https://doi.org/10.1029/2002JD002670.

R Core Team, 2020: R: A language and environment for statistical computing. R Foundation for Statistical Computing, http://www.R-project.org/.

Rodríguez-Fonseca, B., and Coauthors, 2016: A review of ENSO influence on the North Atlantic. A non-stationary signal. *Atmosphere*, **7**, 87, https://doi.org/10.3390/atmos7070087.

Salinger, M. J., J. A. Renwick, and A. B. Mullan, 2001: Interdecadal Pacific oscillation and South Pacific climate. *Int. J. Climatol.*, **21**, 1705–1721, https://doi.org/10.1002/joc.691.

Sánchez-Benítez, A., R. García-Herrera, D. Barriopedro, P. M. Sousa, and R. M. Trigo, 2018: June 2017: The earliest European summer mega-heatwave of reanalysis period. *Geophys. Res. Lett.*, **45**, 1955–1962, https://doi.org/10.1002/2018GL077253.

Shaman, J., 2014a: The seasonal effects of ENSO on atmospheric conditions associated with European precipitation: Model simulations of seasonal teleconnections. *J. Climate*, **27**, 1010–1028, https://doi.org/10.1175/JCLI-D-12-00734.1.

——, 2014b: The seasonal effects of ENSO on European precipitation: Observational analysis. *J. Climate*, **27**, 6423–6438, https://doi.org/10.1175/JCLI-D-14-00008.1.

——, and E. Tziperman, 2011: An atmospheric teleconnection linking ENSO and southwestern European precipitation. *J. Climate*, **24**, 124–139, https://doi.org/10.1175/2010JCLI3590.1.

Stockdale, T. N., D. L. T. Anderson, J. O. S. Alves, and M. A. Balmaseda, 1998: Global seasonal rainfall forecasts using a coupled ocean–atmosphere model. *Nature*, **392**, 370–373, https://doi.org/10.1038/32861.

Sutton, R. T., and D. L. R. Hodson, 2003: Influence of the ocean on North Atlantic climate variability 1871–1999. *J. Climate*, **16**, 3296–3313, https://doi.org/10.1175/1520-0442(2003)016<3296:IOTOON>2.0.CO;2.

Takaya, K., and H. Nakamura, 2001: A formulation of a phase-independent wave-activity flux for stationary and migratory quasigeostrophic eddies on a zonally varying basic flow. *J. Atmos. Sci.*, **58**, 608–627, https://doi.org/10.1175/1520-0469(2001)058<0608:AFOAPI>2.0.CO;2.

Taschetto, A. S., C. C. Ummenhofer, M. F. Stuecker, D. Dommenget, K. Ashok, R. R. Rodrigues, and S. Yeh, 2020: ENSO atmospheric teleconnections. *El Niño Southern Oscillation in a Changing Climate, Geophys. Monogr.*, Vol. 253, Amer. Geophys. Union, 309–335, https://doi.org/10.1002/9781119548164.ch14.

Teng, H., and G. Branstator, 2019: Amplification of waveguide teleconnections in the boreal summer. *Curr. Climate Change Rep.*, **5**, 421–432, https://doi.org/10.1007/s40641-019-00150-x.

Trigo, R. M., R. García-Herrera, J. Díaz, I. F. Trigo, and M. A. Valente, 2005: How exceptional was the early August 2003 heatwave in France? *Geophys. Res. Lett.*, **32**, L10701, https://doi.org/10.1029/2005GL022410.

Vecchi, G. A., and B. J. Soden, 2007: Global warming and the weakening of the tropical circulation. *J. Climate*, **20**, 4316–4340, https://doi.org/10.1175/JCLI4258.1.

Venrick, E. L., J. A. McGowan, D. R. Cayan, and T. L. Hayward, 1987: Climate and chlorophyll a: Long-term trends in the

central North Pacific Ocean. *Science*, **238**, 70–72, https://doi.org/10.1126/science.238.4823.70.

Vicente-Serrano, S. M., and E. Rodríguez-Camino, 2017: Observed atmospheric trends in the Iberian Peninsula. *CLIVAR Exchanges*, No. 73, International CLIVAR Project Office, Southampton, United Kingdom, 20–23.

von Storch, H., and W. F. Zwiers, 2001: *Statistical Analysis in Climate Research*. Cambridge University Press, 484 pp.

Wang, H., B. Wang, F. Huang, Q. Ding, and J. Y. Lee, 2012: Interdecadal change of the boreal summer circumglobal teleconnection (1958–2010). *Geophys. Res. Lett.*, **39**, L12704, https://doi.org/10.1029/2012GL052371.

Woollings, T., and M. Blackburn, 2012: The North Atlantic jet stream under climate change and its relation to the NAO and EA patterns. *J. Climate*, **25**, 886–902, https://doi.org/10.1175/JCLI-D-11-00087.1.

Yu, B., X. Zhang, H. Lin, and J. Y. Yu, 2015: Comparison of wintertime North American climate impacts associated with multiple ENSO indices. *Atmos.–Ocean*, **53**, 426–445, https://doi.org/10.1080/07055900.2015.1079697.

Zanchettin, D., S. W. Franks, P. Traverso, and M. Tomasino, 2008: On ENSO impacts on European wintertime rainfalls and their modulation by the NAO and the Pacific multi-decadal variability described through the PDO index. *Int. J. Climatol.*, **28**, 995–1006, https://doi.org/10.1002/joc.1601.

Zhang, L., C. Wang, and L. Wu, 2012: Low-frequency modulation of the Atlantic warm pool by the Atlantic multidecadal oscillation. *Climate Dyn.*, **39**, 1661–1671, https://doi.org/10.1007/s00382-011-1257-0.

Zhang, W., Z. Wang, M. F. Stuecker, A. G. Turner, F.-F. Jin, and X. Geng, 2019: Impact of ENSO longitudinal position on teleconnections to the NAO. *Climate Dyn.*, **52**, 257–274, https://doi.org/10.1007/s00382-018-4135-1.

Zheng, J., and C. Wang, 2019: Hot summers in the Northern Hemisphere. *Geophys. Res. Lett.*, **46**, 10 891–10 900, https://doi.org/10.1029/2019GL084219.